

CARBON ENCAPSULATION OF ELEMENTAL NANOPARTICLES

A THESIS SUBMITTED TO  
THE GRADUATE SCHOOL OF NATURAL AND APPLIED SCIENCES  
OF  
MIDDLE EAST TECHNICAL UNIVERSITY

BY

PELİN LİVAN

IN PARTIAL FULFILLMENT OF THE REQUIREMENTS  
FOR  
THE DEGREE OF MASTER OF SCIENCE  
IN  
METALLURGICAL AND MATERIALS ENGINEERING

JULY 2018



Approval of the thesis:

**CARBON ENCAPSULATION OF ELEMENTAL NANOPARTICLES**

submitted by **PELİN LİVAN** in partial fulfillment of the requirements for the degree of **Master of Science in Metallurgical and Materials Engineering Department, Middle East Technical University** by,

Prof. Dr. Halil Kalıpçılar \_\_\_\_\_  
Dean, Graduate School of **Natural and Applied Science**

Prof. Dr. Cemil Hakan Gür \_\_\_\_\_  
Head of Department, **Metallurgical and Materials Engineering**

Prof. Dr. Tayfur Öztürk \_\_\_\_\_  
Supervisor, **Metallurgical and Materials Eng. Dept., METU**

**Examining Committee Members:**

Prof. Dr. Kadri Aydınol \_\_\_\_\_  
Metallurgical and Materials Engineering Dept., METU

Prof. Dr. Tayfur Öztürk \_\_\_\_\_  
Metallurgical and Materials Engineering Dept., METU

Prof. Dr. Hatem Akbulut \_\_\_\_\_  
Metallurgical and Materials Engineering Dept., Sakarya University

Assist. Prof. Dr. Simge Çınar \_\_\_\_\_  
Metallurgical and Materials Engineering Dept., METU

Assist. Prof. Dr. Mert Efe \_\_\_\_\_  
Metallurgical and Materials Engineering Dept., METU

**Date:** 27/07/2018

**I hereby declare that all information in this document has been obtained and presented in accordance with academic rules and ethical conduct. I also declare that, as required by these rules and conduct, I have fully cited and referenced all material and results that are not original to this work.**

Name, Last name : Pelin Livan

Signature :

## **ABSTRACT**

### **CARBON ENCAPSULATION OF ELEMENTAL NANOPARTICLES**

Livan, Pelin

MSc., Department of Metallurgical and Materials Engineering

Supervisor: Prof. Dr. Tayfur Öztürk

July 2018, 57 pages

There is a considerable interest in the encapsulation of nanoparticles into the carbon cages for a variety of purposes e.g. providing stability in detrimental environments, preventing agglomeration, controlling surface modifications and improving in electrical conductivity etc. The current study deals with the encapsulation of elemental particles and is made up of two parts.

In the first part, the encapsulation of elemental particles was studied using a spark discharge generator where an elemental rod used against a carbon electrode under a constant argon flow. The source of carbon was further enriched by methane which was co-fed with argon into the reaction chamber. The study showed that elements W, V, Ti and Si were converted into carbide and were encapsulated successfully by graphitic layers producing sound core-shell structure. Cu yielded a partially filled core-shell structure. The resulting structure in the case of Mg was quite different. Here Mg did not produce encapsulated structure; rather it occurred as elemental particles embedded in graphitic matrix. Simple calculation based on empty volume in the partially filled Cu core-shell structure indicated that the process of encapsulation is probably complete at around 1900 K. Considering that carbon condenses at around 4000 K, elements may be divided into three categories. Elements/carbides with condensation temperature higher than 4000 K e.g. W, V or Ti produce a sound core-shell structure. Elements/carbides whose condensation

temperature is between 4000 K and 1900 K yield sound or partially filled core-shell structure depending on the volume shrinkage during solidification. Elements/compounds whose condensation temperature is below 1900 K fail to develop core-shell structure. Instead, they form embedded composite structure where particles are embedded into a graphitic matrix.

In the second part of this study, encapsulation of silicon nanoparticles was studied by thermal plasma. Feeding Si powders together with methane into a 25 kW RF reactor yielded nanopowders which comprised SiC, Si, and graphite. The particles were successfully encapsulated with 7-10 nm thick graphitic layers with a high degree of crystallinity. Co-feeding of silicon with methane therefore did not yield pure Si@C as carbide formation was unavoidable. It is proposed that it might be possible to obtain Si@C i.e. carbon encapsulated Si nanoparticles, but for this an alternative approach may be adopted, i.e. first to produce Si nanoparticles and encapsulating them by post feeding of methane at lower temperature.

Keywords: Carbon encapsulation, Core- Shell Structure, Spark Discharge, RF induction thermal plasma, Elemental nanoparticles, Silicon Nanoparticle

## ÖZ

### ELEMENTEL NANOPARÇACIKLARIN KARBON İLE ENKAPSÜLASYONU

Livan, Pelin

Yüksek Lisans, Metalurji ve Malzeme Mühendisliği Bölümü

Tez Yöneticisi: Prof. Dr. Tayfur Öztürk

Temmuz 2018, 57 sayfa

Nanoparçacıkların karbonla kaplanması farklı amaçlar için yapılabilmektedir; parçanın stabilizasyonu, aglomerasyonun engellenmesi ve elektriksel iletkenliğin artırılması vb. Elementel nanoparçacıkların enkapsüle edilmesini konu alan mevcut çalışma iki kısımdan oluşmaktadır.

İlk kısımda, enkapsülasyon kıvılcım boşaltma yöntemi ile sabit bir argon akışı altında karbon elektroda karşı saf element bir elektrot kullanılmak sureti ile gerçekleştirildi. İlave olarak reaksiyon haznesine metan gazı beslenmek sureti ile kıvılcım karbonca zengin bir ortamda gerçekleştirildi. Çalışma W, V, Ti ve Si elementlerinin karbür haline dönüştüğünü ve grafit tabakaları ile başarılı bir şekilde enkapsüle edildiğini gösterdi. Cu durumunda elementin karbüre dönüşmediği ve başarılı bir şekilde enkapsüle olmakla beraber kapsülün tam dolu olmadığı yaklaşık 1/3'lük bir hacmin boş olduğu gözlemlendi. Mg durumunda ise yapının tamamen farklı olduğu tespit edildi. Bu yapıda Mg parçacıklarının enkapsüle olmadığı ancak oluşan karbon esaslı ana yapı içerisinde gömülü parçacıklar olarak oluştuğu tespit edildi. Cu kapsülün içerisindeki boş hacminin enkapsülasyon işlemi sonrasında gerçekleşen katılaşmanın bir sonucu olduğu varsayılarak enkapsülasyon işleminin 1900 K civarında tamamlandığı sonucuna varıldı. 1900 K enkapsülasyon sıcaklığı ve karbonun 4000 K de yoğunlaştığı esas alınarak enkapsülasyonda 3 kategori

tanımlamanın mümkün olduđu belirtildi. Yoğunlaşma sıcaklığı 4000 K sıcaklığından yüksek olan W, V ve Ti vb. elementler/karbürler tam çekirdek-kabuk yapısını göstermektedir. Yoğunlaşma sıcaklığı 4000 K ve 1900 K arasında olan elementler/karbürler ise katılma sürecindeki hacim daralmasına bağılı olarak tam ya da kısmen dolu çekirdek-kabuk yapısına sebep olmaktadır. Yoğunlaşma sıcaklığı 1900 K sıcaklığının altında olan elementler/karbürler ise çekirdek-kabuk yapısını oluşturamamakta bunun yerine gömülü olduđu kompozit bir yapı oluşturmaktadırlar.

Çalışmanın ikinci bölümü ise karbon ile enkapsüle edilmiş silikon nanoparçacıklarını RF termal plazma ile üretim konu almaktadır. Bu amaçla Si tozları metan ile birlikte 25 kWlık bir RF reaktörüne beslenmiş ve sonuçta SiC, Si ve grafit içeren nano tozlar elde edilmiştir. İşlem başarılı olmuş ve sonuçta parçacıkların 7-10 nm kalınlığında grafit tabakaları ile enkapsüle edilmiştir. Ancak işlemden SiC oluşumu nedeni ile amaçlanan karbonla kaplı sırf Si parçacıklarından oluşan yapı elde edilememiştir. Bunun için ilk önce Si nano tozlarını üretmenin metanın ise daha düşük sıcaklıklarda beslenerek enkapsülasyon yoluna gidilmesi alternatif bir yaklaşım olarak önerilmiştir.

Anahtar Kelimeler: Karbon enkapsülasyon, Çekirdek- Kabuk yapısı, Kıvılcım Boşaltma Yöntemi, RF İndüksiyon Termal Plazma Yöntemi, Elementel Nanoparçacıklar, Silikon Nanoparçacık

To My Family



## ACKNOWLEDGMENTS

I would first like to express my deepest gratitude to my supervisor Prof. Dr. Tayfur Öztürk for his incredible patience and support in every step of my master studies. During these years, I learned that only one right, act or decision doesn't exist to proceed and importance of integrative thinking will stay with me during my all life path.

I would like to express my feelings about sharing same laboratory with the members of ESM research group Ezgi Onur, Cavit Eyövge, Fatih Pişkin, Doğancan Sarı, Sertaç Altınok and Necmi Avcı. In every struggle, they offered a solution without any doubt. I acknowledge Serkan Yılmaz especially for his help during TEM studies. Also, I am very grateful to Metallurgical and Material department about giving an opportunity to know these valuable people, Yusuf Yıldırım, Arif Atalay Özdemir, Kadir Sevinç and Gülsüm Şahan.

Many thanks go to my precious mother Şayan Livan, father Ali Livan and my big brother Berkin Livan. They support me to come this point during my entire life. Without having any technical knowledge, my friends, Furkan Oğuz, Kadir Uruç, Sezer Çakal, Şirincan Mamak, Sedat Erdoğan, Miraç Eren Aydoğan, Dilan Vargün, Zeynep Elif Koç, Barış Şimşek, Bengisu Akpınar and Berfin Yavuz, listened my every thought throughout these years. Also, I learned so many things during my experience in Poland as an assistant teacher in social care center. For this reason, I would like to thank to my kids in Poland due to their endless joy.

In the end, I was so lucky with all of these people. They are an invulnerable support system for me.



## TABLE OF CONTENTS

ABSTRACT .....	v
ÖZ .....	vii
ACKNOWLEDGMENTS .....	xi
TABLE OF CONTENTS .....	xiii
LIST OF TABLES .....	xiv
LIST OF FIGURES .....	xv
CHAPTERS	
1. INTRODUCTION .....	1
2. SPARK DISCHARGE SYNTHESIS OF CARBON ENCAPSULATED ELEMENTAL NANOPARTICLES .....	5
2.1 Introduction .....	5
2.2 Experimental .....	12
2.2.1 Nanoparticle Synthesis.....	12
2.2.2 Material Characterization.....	14
2.3 Results&Discussion .....	15
2.4 Conclusion .....	26
3. INDUCTION PLASMA SYNTHESIS OF CARBON ENCAPSULATED SILICON NANOPARTICLES .....	29
3.1 Introduction .....	29
3.2 Experimental .....	37
3.2.1 RF Plasma System .....	37
3.2.2 Plasma Reactor.....	39
3.2.3 Material Characterization.....	41
3.3 Results& Discussion .....	41
3.4 Conclusion .....	46
4. GENERAL CONCLUSIONS .....	47
REFERENCES.....	49

## LIST OF TABLES

### TABLES

Table 2. 1 Condensation and melting temperature of elements chosen as cathode material.	13
Table 2. 2 Encapsulation tendency of the elements as determined from the current work supplemented by data from the literature. Elements are ordered according to their condensation temperature. Elements Ta, Nb and Zr whose condensation temperature is greater than C are also included in the table. ....	21
Table 3. 1 Experimental parameters of the RF thermal plasma pyrolysis process of methane. ....	41

## LIST OF FIGURES

### FIGURES

Figure 2. 1 The basic components of the spark discharge generator, chamber and electrical system (Tabrizi <i>et al.</i> 2008). .....	6
Figure 2. 2 Internal and external carbon sources (Elliot <i>et al.</i> 1997).....	9
Figure 2. 3 Vapor pressure curves of rare-earth metals. Elements are divided into their vapor pressures. Sm, Eu, Tm, and Yb are volatile and Sc, Y, La, Ce, Pr, Nd, Gd, Tb, Dy, Ho, Er, and Lu are non-volatile (Saito <i>et al.</i> 1994). .....	10
Figure 2. 4 Schematic drawing of spark discharge generator .....	12
Figure 2. 5 a) Interior design of the spark discharge generator b) graphite electrode (upper) and silicon wafer attached to the copper electrode (bottom). .....	13
Figure 2. 6 Design of the aerosol filter holder. ....	14
Figure 2. 7 a) collected silicon nanoparticles on the filter. b) silicon nanoparticles after the ultrasonicated in the ethanol. ....	15
Figure 2. 8 TEM images of the a) particles produced with a spark discharge generator. b) Nanoparticle covered with 20-25 graphitic layers. Insets show a close-up image from the core and also it's FFT. ....	16
Figure 2. 9 TEM images of the distinct core shell structure obtained from the spark discharge process of a) vanadium and b) titanium electrodes. Insets shows FFT image of the core regions.....	17
Figure 2. 10 TEM images of the a,b) partially filled copper core shell structure. c) the surface of an encapsulated particle for the silicon electrode d) silicon nanoparticle encapsulated in carbon cages. Inset shows FFT images of the core regions. ....	18
Figure 2. 11 TEM images of the nanoparticles embedded in carbonaceous matrix obtained from the spark discharge process of magnesium. Inset shows FFT images of the crystalline regions.....	19
Figure 2. 12 Regions of different encapsulation behavior. Elements are ordered based on their condensation temperature. Region I yield a sound core-shell structure and cover elements/compounds whose condensation temperature is greater than that of carbon (graphite). Horizontal line drawn at 1900 K is the estimated temperature for carbon shell formation. Elements in Region II might yield sound or partially filled core-shell structure-see legends under the figure. Region III covers elements whose condensation temperature is less that 1900 K and therefore do not encapsulate but yield embedded structure. ....	24
Figure 3. 1 A Schematic of an RF Plasma Torch System Designed for Synthesis of Nano-sized Powders (Seo and Hong 2012). ....	31
Figure 3. 2 a) Schematic of failure mechanism of Si electrode. b) Schematic of SEI formation on a pure silicon surface during charge/discharge cycles (Rahman <i>et al.</i> 2016)...	35
Figure 3. 3 Schematic of the tubular reactor equipped with two radio frequencies, capacitive-coupled plasma sources used to synthesize carbon-coated silicon nanoparticles (Chaukulkar <i>et al.</i> 2014). ....	36
Figure 3. 4 Schematic design of RF induction thermal plasma system (Aktekin <i>et al.</i> 2014). ....	38

Figure 3. 5 a) Actual design of the bottom collector, cyclone collector, powder collector, respectively. Actual view from the collection unit of the b) bottom collector c) cyclone collector d) powder collector. ....	39
Figure 3. 6 a) Schematic diagram of the RF induction thermal plasma system. b) Photograph of the plasma torch.....	40
Figure 3. 7 Rietveld refinement of the X-ray diffractogram of powder synthesized by induction thermal plasma. ....	42
Figure 3. 8 Raman spectra of samples obtained by induction thermal plasma process. ....	43
Figure 3. 9 a) Low magnification TEM images of the nanoparticles and carbon nanostructures. b) Low magnification TEM images of the core/shell structure. ....	43
Figure 3. 10 High-resolution TEM image of the graphitic shell, showing a layered structure. Inset is the FFT image.....	44
Figure 3. 11 HRTEM image of the interface between nanoparticle and carbon cage. Insets show a close-up image from the carbon cage and its FFT image. ....	45

## CHAPTER 1

### INTRODUCTION

Nanoparticles have an important role in a wide variety of applications including catalysts, solar technology and energy conversion and storage. Large surface to volume ratio, quantum mechanics size effects and curvature induced surface effects of these particles brings novel physical and chemical properties. However, large specific surface area and high chemical reactivity of nanoparticles lead the difficulties, e.g. surface oxidation and agglomeration, in the processing of these materials (Yin and Talapin 2013, Conte *et al.* 2004).

The case of magnetic nanoparticles (Fe, Co and Ni) constitutes a good example. These are important in a wide range of areas such as magnetic data storage, sensors and targeted drug delivery systems but rapid oxidations of these particles changes the character of particles resulted from the creation of thin oxide layers (Bystrzejewski *et al.* 2011). Another example is silicon used as anode in Li-ion batteries. Due to their very high surface-to-volume ratio, silicon nanoparticles offer more contact with the current collector in the electrode. Moreover, volume expansion of these nanoparticles will be small during charging and discharging and thus breakup of structure will be decrease while obtaining long battery life (Ashuri *et al.* 2016).

Among the various protection strategies, encapsulation of nanoparticles into the protective cages has been special interests especially in recent years. Since these composite particles are constructed of cores and shells of different chemical compositions. In this way, it combines the different properties in the same particle. Firstly, encapsulation process preserves the intrinsic properties of nanoparticles. Also, having a strong resistance of cage structure against degradation solve limitations in the processing of nanoparticles (Seraphin *et al.* 1996).

Shell materials used for encapsulation involve polymers, e.g., (polyelectrolytes (Shin and Jang 2007)), oxides (e.g., SiO<sub>2</sub>, SnO<sub>2</sub> or TiO<sub>2</sub> (Sim *et al.* 2013, Lipp and Pletcher 1997, Fu *et al.* 2005)) as well as C (Tomita *et al.* 1993). Especially, oxides which are transparent and chemically stable were chosen as the shell materials where the purpose is protection. For example, Niu *et al.* (2015) produced Si@SiO<sub>2</sub> i.e. Si core and SiO<sub>2</sub> shell, by solution based method to be used as anode material for lithium ion batteries.

Among the possible shell materials, carbon has a special place. High stability of carbon in severe environments such as in acids, bases as well as high temperatures provides protection to the core material against degradation and agglomeration. Also, having variable functional groups of carbon layers allows controlled surface modifications. An important advantage of carbon encapsulation is improved conductivity of the encapsulated particles and as a result it was made use of extensively since many of the electrode materials have insufficient conductivity (Zhang *et al.* 2013).

Following the first report by Kratschmer and Huffman (1990) on a simple method for generating fullerenes by carbon arc method, many reports have been published on synthesis and properties of carbon encapsulates. Tomita *et al.* (1993) reported that arc discharging carbon rods containing 8.8 wt. % La<sub>2</sub>O<sub>3</sub> produces a carbonaceous deposit containing nanoparticles consisting of graphitic shells. Following the success of initial study, many of rare earth elements, Sc, Y, La, Pr, Nd, Gd, Tb, Dy, Ho, Er, Lu, Sm, Eu and Yb, were encapsulated by Saito *et al.* (1994) to solve the degradation problems, arising from their hygroscopicity.

Many of the rare earth metals were encapsulated quite successfully using arc discharge. This was, however, except for Sm, Eu and Yb. Factors affecting the success of encapsulation were subject of considerable interest in the 90's. One explanation advanced by Saito *et al.* (1994) as to why Sm, Eu and Yb failed to encapsulate was related to high vapour pressure of these elements. An alternative

explanation was advanced by Guerret-Piécourt *et al.* (1994) based on the electronic structure of elements. Elliot *et al.* (1997) in the same context put forward a detailed explanation of the encapsulation process. According to this study, there are two local sources of carbon internal and external which can be active separately or simultaneously; during cooling, internally contained carbon within the clusters expelled to the surface forming the encapsulate. Externally carbon which is present condenses onto the already formed particles resulting in encapsulation.

Research in the subsequent period has covered the other elements and alternative synthesis methods. Thus, various magnetic materials Fe, Co, Ni, FeCo, Fe<sub>x</sub>O<sub>y</sub> and Fe-Nd-B (Bystrzejewski *et al.* 2011, Dravid *et al.* 1995, Seshadri *et al.* 1994, Lee *et al.* 2011, Yu *et al.* 2010 and Wozniak *et al.* 2006) were encapsulated into carbon cages to enhance their magnetic properties via arc discharge using either carbon electrode (Chaitoglou *et al.* 2014) or ethanol (Si *et al.* 2013) or methane vapour (Jiao and Seraphin 1998) as carbon source. Alternative synthesis method used included thermal plasma (Bystrzejewski *et al.* 2011), flame synthesis (Athanasidou *et al.* 2006), laser ablation (Zhang *et al.* 2013), chemical vapour deposition (Liu *et al.* 2001) and hydrothermal reactions (Xuan *et al.* 2007). Of the elements studied in recent years, Si has attracted considerable interest because of its potential as anode material for li-ion batteries. Many studies were conducted which made use of solution based method (Liu *et al.* 2012, Zhou *et al.* 2013) yielding the encapsulated structure. Thermal route was also used where attempts were made to encapsulate Si nanoparticles with carbon (Chaukulkar *et al.* 2014).

The current study was divided into two parts. In the first part, a systematic study was carried out to investigate the carbon encapsulation of a wide range of elements so as to determine the capability of the process to yield the encapsulated products. For this purpose, of the thermal methods, a spark discharge method was preferred as this was quite simple and an easily operated process. In the second part, the study was focused on carbon coating of silicon nanoparticles using RF thermal plasma.



## CHAPTER 2

### SPARK DISCHARGE SYNTHESIS OF CARBON ENCAPSULATED ELEMENTAL NANOPARTICLES

#### 2.1 Introduction

<sup>1</sup>In this chapter, motivated by general advantages of particle synthesis in the gas phase, carbon encapsulated elemental nanoparticles coming were synthesized by spark discharge technique. It is a physical method of generating aerosol which involve evaporation, condensation and the transport of nanoparticles. The use of spark discharge as a method of aerosol production has several advantages compared to other methods. It is simple and proper for scale up production (Roth *et al.* 2004). Additionally, range of nanoparticles with a high purity can be produced with this method. Synthesis of monodisperse carbon and gold nanoparticles were the initial studies in this field (Schwyn *et al.* 1988). However, the method was expanded into a broad range covering any conductive materials as well as the semiconductors (Cole *et al.* 2009).

In order to generate nanoparticles via spark discharge, an apparatus is necessary to comprise a chamber comprising the electrodes with controlled atmosphere and an electric circuit to control the spark generation, see Figure 2.1. The spark is generated between the two electrodes separated by a gap. The two electrodes can be prepared either from the same material or from different materials. A high voltage power supply coupled with a capacitor is connected to the electrodes. When the capacitor reaches a breakdown voltage which depends on the gap and the atmosphere (carrier gas), a spark is generated across the electrodes. This evaporates the material from the electrodes and an aerosol is formed with argon maintained into the chamber. If the

---

<sup>1</sup> This chapter is based on a paper entitled “Carbon encapsulation of elemental nanoparticles by spark discharge” J of Materials Science, 53(20) (2018) 14350–14360.

electrodes used are of different materials, a composite aerosol will form. The aerosol is transported out of the chamber via flowing argon.

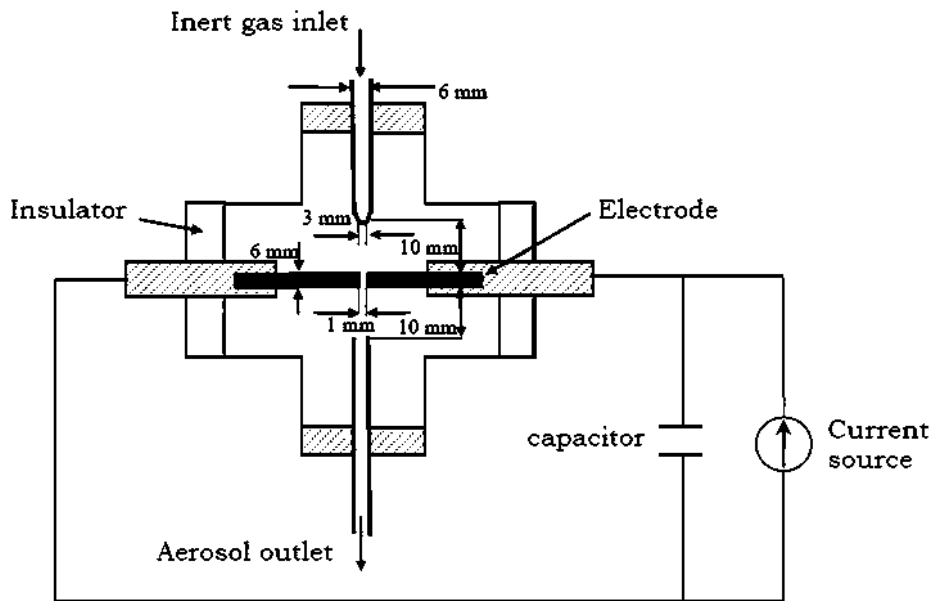


Figure 2. 1 The basic components of the spark discharge generator, chamber and electrical system (Tabrizi *et al.* 2008).

The generated spark leads to very high local temperature (up to between 20000 K and 30000 K) (Tabrizi *et al.* 2008). Following the evaporation of electrode material resulted from the high temperatures, electrode material occur in a gaseous form. The evaporated electrode material in the supersaturated cloud will then nucleate and yield stable particles via condensation.

There are several parameters that effect the operation of the generator. These include inter electrode gap, capacitance, electrode material and spark frequency as well as gas maintained across the gap, together with its pressure and flow rate (Meuller *et al.* 2012).

Also, gases have a huge effect on particle formation mechanism. Different cooling effect of gases with the metal vapor affects the particle formation. Meuller *et al.* (2012) showed that primary particles produced under N<sub>2</sub> were somewhat larger than those produced in the other gases e.g. Ar or He. Gas flow rate have an effect on the rate of cooling during the condensation and therefore affects the resulting particle size.

Schwyn *et al.* (1988) used the spark generator to produce carbon and gold nanoparticles from the electrodes of the same material in a N<sub>2</sub> atmosphere. They were able to produce carbon aerosol with a low impurity content using carbon electrodes. Also, charged gold particles in a 1.3 nm sized range have been produced when carbon electrodes were replaced by gold electrodes in the same atmosphere and power conditions.

After this initial study, spark discharge generator was expanded into generation of monometallic nanoparticles from electrodes of the same materials. These include gold (Messing *et al.* 2009), nickel, platinum (Seipenbusch *et al.* 2003), palladium (Messing *et al.* 2010), rhodium (Blomberg *et al.* 2014), copper, tin, lead (Lafont *et al.* 2009), silver (Guo *et al.* 2015), iron, cobalt, titanium (Jiao and Seraphin 1998) and magnesium (Aktekin, 2013). Byeon *et al.* (2008) generating (Pd), Platinum (Pt), Gold (Au) and Silver (Ag) nanoparticles obtained nanoparticles which were in the form of agglomerates of 14.9, 26.7, 37.7 and 48.8 nm, in the respective order. The individual particles making up the agglomerates were 2 to 4 nm.

Vons *et al.* (2011) have used silicon electrodes, intrinsic silicon rods. They successfully obtained unoxidised silicon nanoparticles with a primary particle size of 3-5 nm.

Also, metal oxides can also be produced by the spark discharge generator. This is normally achieved by maintain a small rate of oxygen flow to the chamber in addition to the main gas of argon. Examples of metal oxide nanoparticles generated by the spark discharge generator method are iron oxide, copper oxide (Evans *et al.* 2003), zinc oxide, cadmium oxide (Kim and Chang 2005) and titanium oxide (Kreyling *et al.* 2011). Kim and Chang (2005) in their study have used two copper electrodes across which an air flow was maintained from 3 to 15 l/min together with Ar. They obtained oxide particles of 2-4 nm.

Nanoparticles consisting of mixed elements have also been generated by the spark discharge generator method. This could be achieved by using pre-alloyed electrodes or two electrodes of different materials. Examples include mixtures of carbon-iron, copper-zinc, copper- nickel (Tabrizi *et al.* 2009), palladium- platinum, gold-silver,

chromium–cobalt (Blomberg *et al.* 2013) and magnesium with titanium (Anastasopol *et al.* 2013).

In a similar study, Tabrizi *et al.* (2010) have synthesized Ag-Cu, Pt- Au and Cu-W mixed particles which were several nanometer in size. TEM, XRD and EDS analysis give evidence of mixing of elements on a subnanometer scale.

Finally, nanoparticles in the form of core shell structure were also produced with spark discharge generator. Most of rare earth metals (La (Tomita *et al.* 1993) ,Sc, Y, Ce, Pr, Nd, Gd, Tb, Dy, Ho, Er and Lu (Saito *et al.* 1994, Seraphin *et al.* 1996) and 3-d transition metals especially Fe, Co and Ni (Si *et al.* 2003, Jiao and Seraphin 1998), important for their magnetic properties could be covered with carbon shells using this method. The core-shell structure in these studies were obtained using either two carbon electrodes one of which was drilled and filled with the core metal or one graphite electrode used against the core electrode.

Guerret-Piecourt *et al.* (1994) suggested that encapsulation behavior depends on the electronic configuration of the metal. According to the study, encapsulation behavior of metals in the most stable ionic state can be determined by incomplete electronic shell configuration. However, they understood that Mo and Pd can be encapsulated but they do not have a complete electronic shell. Majetich *et al.* (1994) suggested that the encapsulation cannot be observed for the materials having a low melting point. However, studies of Seraphin *et al.* (1997) revealed that hypothesis cannot be used to explain results of metals that do not form carbides, e.g. Ag, Cu, Pd. Also, Mn having a low melting point was encapsulated in carbon cages.

Elliot *et al.* (1997) predict the encapsulation behavior of elements in the concept of core material formed in elemental or carbide. According to the rule, elements having stable carbide at room temperature prefer the formation of encapsulated core shell structure. However, consumption of carbon can be resulted with the inhibition of shell structure. A study covering a wide range of elements in the literature (B, Cr, Gd, La, Mn, Mo, Nb, Si, Ti, V, Y,W and Zr) indicate that there is a struggle to prevent stable carbide phase formation during an arc process with carbon source. If

observation of metal cores is a aim of process, metals which does not have a stable carbide phase have to be used for process (Co, Cu, Fe, Ni, and Pd).

In the same study, investigation of encapsulation mechanism was done. According to Elliot *et al.* (1997) there are only two local sources of carbon; internal and external (Fig. 2.2). Following the crystallization process of nanoparticles, surface diffusion of carbon expelled from the core region as an excess part occurs. In this way, metal or carbide core is encapsulated. Activation process of internal and external carbon sources can be proceed together. This means that graphite can be deposited on the surface by an external carbon source and simultaneous expulsion of excess carbon to the surface.

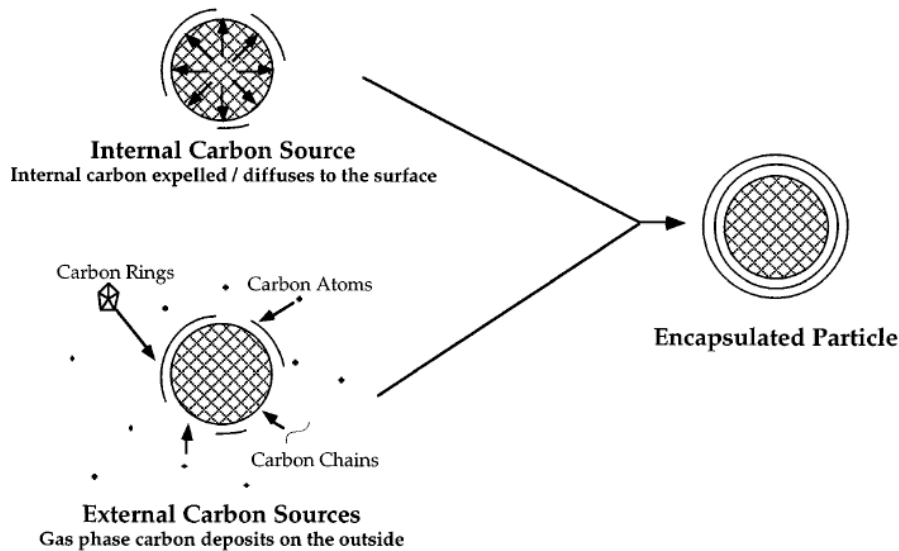


Figure 2. 2 Internal and external carbon sources (Elliot *et al.* 1997).

Core-shell structure can also be produced via spark-discharge. Tomita *et al.* (1993) using carbon rods containing 8.8 wt%  $\text{La}_2\text{O}_3$  produced a carbonaceous deposit containing nano-particles ranging from 3-4 to 10-30 in size with graphitic shells. Their TEM investigation showed that the core formed from LaC was encapsulated with the graphitic layers. Saito *et al.* (1994) showed that the most of rare earth metals (Sc, Y, La, Ce, Pr, Nd, Gd, Tb, Dy, Ho, Er and Lu) similarly produced carbides that are encapsulated with graphite. Elements Sm, Eu and Yb were, however, different which did not develop a core-shell structure. In this study, graphite electrode was

used against the metal loaded graphite electrode with helium flow. According to this study, the vapor pressure of elements can be used as a determining factor for encapsulation tendency of elements. Figure 2.3 is taken from their study which shows the variation of vapor pressure of rare earth elements as a function of temperature. They stated that the volatility of the elements affect the process of metal encapsulation. Rare earth elements that are successfully encapsulated belong to group of relatively low vapor pressure. Elements such as Sm, Eu were not encapsulated due to their high vapor pressure.

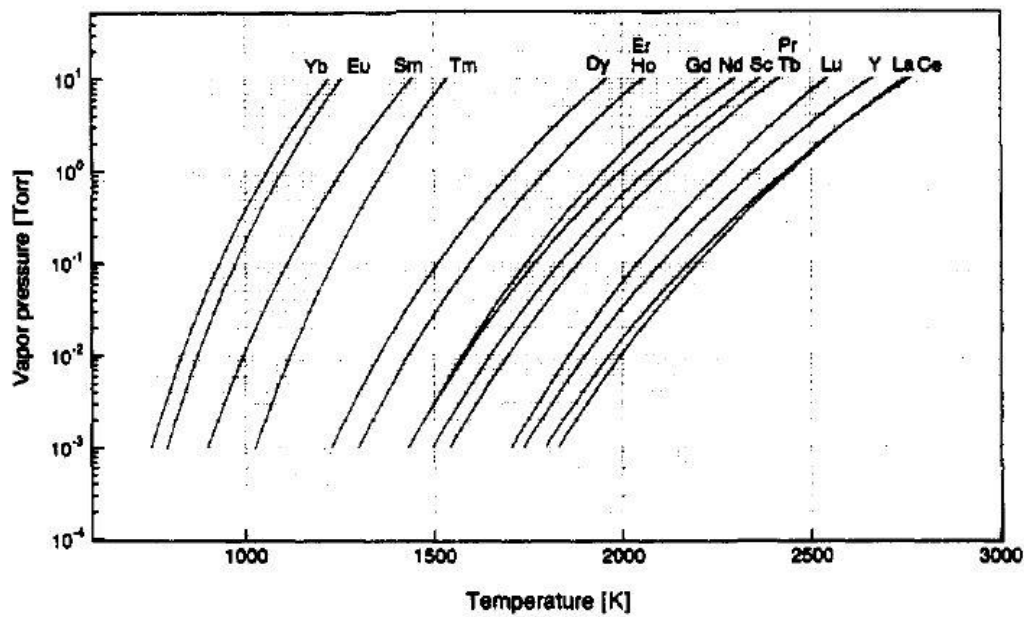


Figure 2. 3 Vapor pressure curves of rare-earth metals. Elements are divided into their vapor pressures. Sm, Eu, Tm, and Yb are volatile and Sc, Y, La, Ce, Pr, Nd, Gd, Tb, Dy, Ho, Er, and Lu are non-volatile (Saito *et al.* 1994).

For the transition metals Si *et al.* (2003) have successfully obtained carbon coated iron and nickel nanocapsules with the size of 6-40 nm and 30-70 nm, respectively. In this study one of the electrodes was carbon but carbon source was enriched by adding liquid alcohol into the chamber together with argon. High resolution transmission electron microscopy imaging showed that the structure in the form of core/shell. In this study, they also observed two particles sharing a common shell.

Jiao and Seraphin (1998) have used methane as a carbon source fed into the chamber together with a carbon electrode and obtained core-shell particles of Ni, Co, Cu.

Also, encapsulation of Ti was achieved but the core was in the form of carbide. Synthesis powders were annealed at elevated temperatures and process resulted with the increasing number of encapsulating layers. However, annealing process of Ti resulted with the same number of layer, i.e. 1-2 layers.

Seraphin *et al.* (1996) divided elements into four groups as a result of systematic study covered arc discharge process of twenty elements. B, V, Cr, Mn, Y, Zr, Nb, Mo belongs to first group and carbide core formation was observed. Following this, second group elements, Cu, Zn, Pd, Ag and Pt, were not encapsulated but empty graphitic cages were observed in the structure. Stable carbide former elements, Al, Si, Ti, W, compete with and pre-empting the carbon supply for the graphitic cage formation. The iron-group metals, Fe, Co, Ni that promote the encapsulation process according to results, there is a relationship between carbide formation and encapsulation behavior of elements. In the absence of thermodynamically stable carbide phase, encapsulation is not observed but cages formation can be possible. On the contrary, cage formation can be prohibited in the case of absence of extra carbon atom resulted from the carbide core. However, there is an exception in the case of encapsulation process of Zr which is strong carbide former element. It resulted with the formation of encapsulated core structure. Also, successful encapsulation expected in the case of Al, Si, W due to the carbide formation tendency but process was not achieved. They suggest that the in addition to the physical properties of elements such as vapor pressure, melting and boiling points, the completeness of the electronic shells of the elements, or their heat of carbide formation, other parameters have to be considered to more depth understanding of encapsulation behavior of elements.

In summary, spark discharge generation is a highly versatile method for production of nanoparticles of a wide range of different materials including carbon, metals, alloys and metal oxides. The method is also suitable for the synthesis of core-shell structures. And we used for this purpose for metals including different elemental groups.

## 2.2 Experimental

### 2.2.1 Nanoparticle Synthesis

Carbon encapsulation of metal nanoparticles was carried out in a spark discharge generator. Palas GFG-100, aerosol generator was adapted for this purpose. A schematic drawing of the generators is given in Figure 2.4. This comprises a high voltage power supply (230 V) coupled with a capacitor with required electronics that allow the frequency of the discharge to be controlled. The main feature of the system is that the gap between the electrodes was adjusted automatically during discharge process. This feature enables continuous operation of the generator over long periods of time without the need for adjustments.

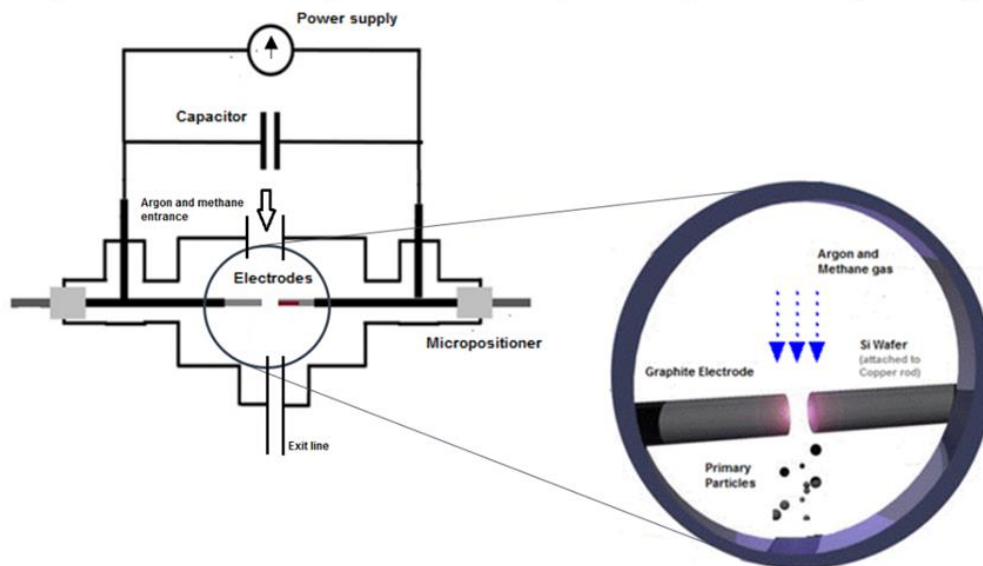


Figure 2. 4 Schematic drawing of spark discharge generator

The generator comprises a chamber accommodating two facing electrodes. One of the electrodes was pure graphite rod, 6 mm in diameter, 100 mm in length connected as cathode to the generator, Figure 2.5(a). The other electrode was a pure metal rod of the same size. Situation was except for silicon for which 1 mm thick, silicon (p-type) the size of 10x6 mm was placed in a copper rod into a slot, cut at its end, facing the graphite electrode. Thus silicon formed a protrusion from the copper rod, Figure 2.5(b). In this configuration, Cu has no role in discharge processes and act

only as the anode holder. Physical parameters of elements used as a cathode material is given in Table 2.1.

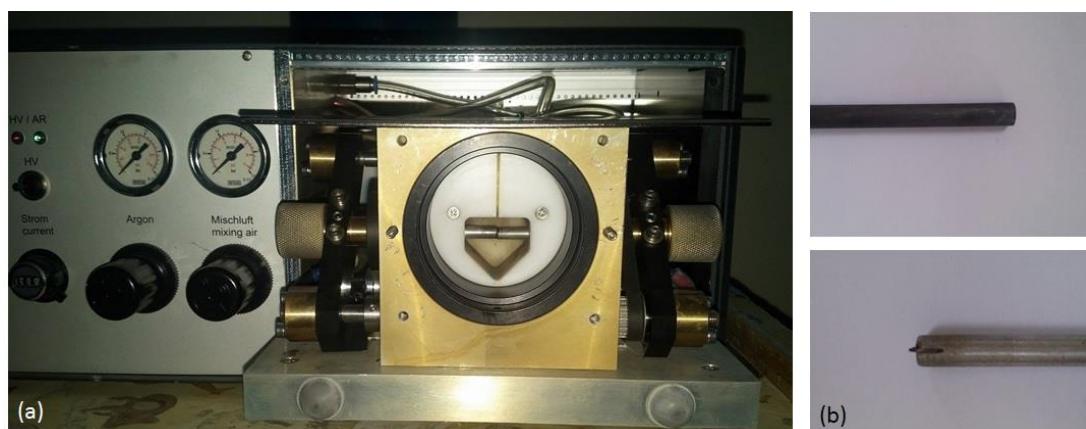


Figure 2. 5 a) Interior design of the spark discharge generator b) graphite electrode (upper) and silicon wafer attached to the copper electrode (bottom).

Table 2. 1 Condensation and melting temperature of elements chosen as cathode material.

Material	Condensation Temperature ( $T_b$ , K)	Melting Temperature ( $T_m$ , K)
Tungsten (W)	5933.15	3683.15
Vanadium (V)	3653.15	2163.15
Titanium (Ti)	3560.15	1933.15
Silicon (Si)	2628.15	1683.15
Copper (Cu)	2840.15	1356.15
Magnesium (Mg)	1380.15	923.15

The reactor had an inlet facing the gap between the electrodes through which argon flow was maintained at a rate of 2.0 sl/min. Argon was mixed with methane gas at a rate of 0.6 sl/min to provide an additional source of carbon. Aerosol generated leave the chamber at the exit transported via the line and collected with a suitable filter (Pallflex), (Figure 2.6).



Figure 2. 6 Design of the aerosol filter holder.

Parameters of operations in the spark generator were constant; a gas pressure of 1.5 bar was maintained at the chamber with a gas flow rate of 2.6 sl/min and frequency of spark generations was of  $200\text{ s}^{-1}$ . The duration of experiments was 8 hours.

### **2.2.2 Material Characterization**

Nanoparticles collected onto the filter were separated from the filter. For this purpose, the filter was dipped into ethanol and ultra sonicated for 5 minutes, Figure 2.7. After 10 minutes at rest, 1-2 droplets of this liquid were dropped on a 200 mesh copper holey carbon grid.

Nanoparticles obtained in this were examined in Jeol JEM2100F Field Emission Transmission Electron Microscope. Necessary FFT images were obtained using GMS3 software. Normally particles were examined with regard to their morphology and the presence or absence of encapsulation. Necessary d-spacing were measured from the lattice imaging.

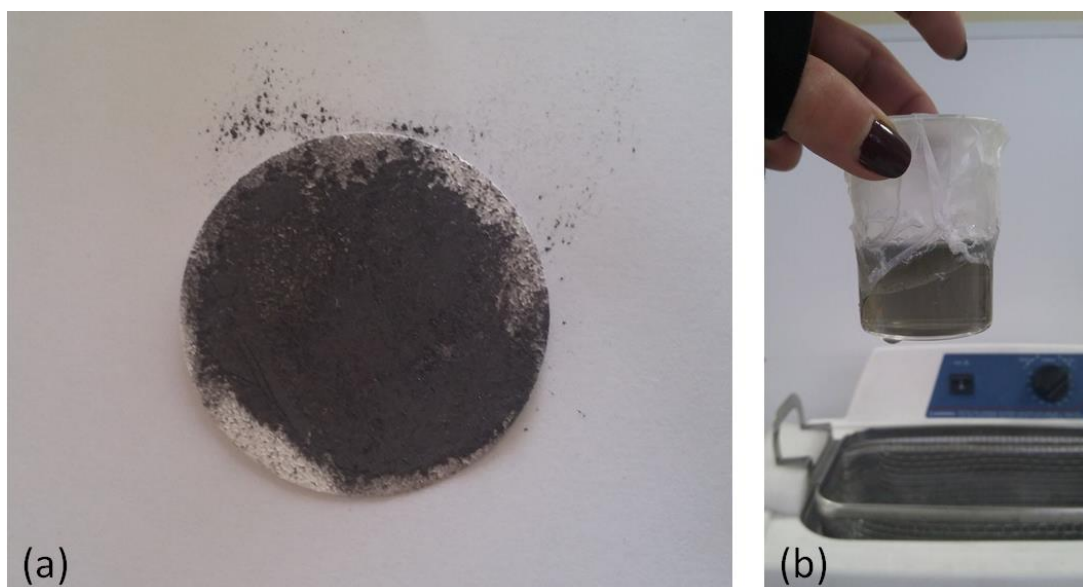


Figure 2. 7 a) collected silicon nanoparticles on the filter. b) silicon nanoparticles after the ultrasonicated in the ethanol.

### 2.3 Results&Discussion

Encapsulation of metallic nanoparticles was examined for a range of elements. These covered elements such as Mg and Si and many were transition elements namely Ti, V, Cu and W. It should be mentioned that elements Ti, V, W and Si are stable carbide formers whereas the other metals Mg and Cu do not.

A typical TEM micrograph of W nanoparticles synthesized by spark discharge is given in Figure 2.8. A range of particle size is 5-10 nm but occasionally particles as large as 75 nm. Small particles were encapsulated by 8-10 layers whereas larger ones the numbers of layers were more. Lattice imaging measurement of inter graphitic distance verify that they are graphite. Also, FFT images taken from the core region consisted with the (001) plane of WC.

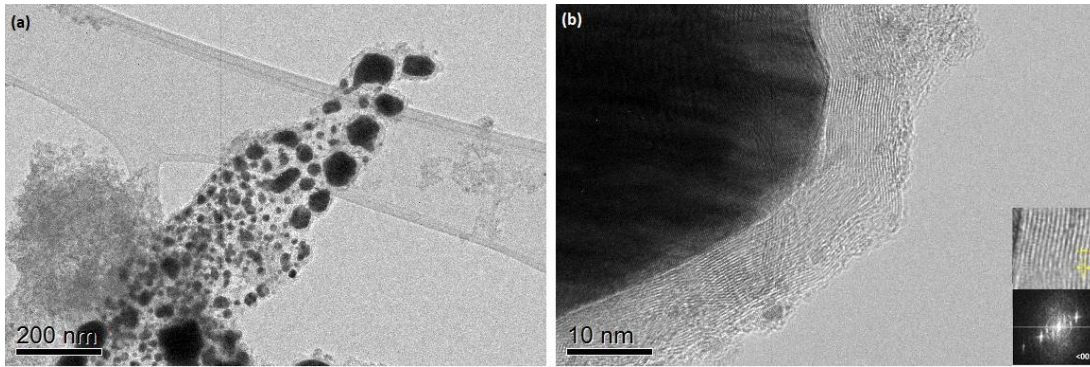


Figure 2. 8 TEM images of the a) particles produced with a spark discharge generator. b) Nanoparticle covered with 20-25 graphitic layers. Insets show a close-up image from the core and also it's FFT.

A TEM image of the vanadium particles is shown in Figure 2.9(a). The core structure is encapsulated in polyhedral concentric graphitic shells with a varying number of layers. The thickness of coating around the core structure (50 nm sized) was about 3.6 nm. The interlayer distance between graphene layers was about 0.339 nm, which is close to the distance in well crystallized graphite. Diffraction pattern from the core region showed that vanadium particles encapsulated in the carbide form. It consisted with the (111) plane of VC. Nearly same morphology observed for the titanium elements. (Figure 2.9(b)). Particle size is smaller than 10 nm. Encapsulation of nanoparticles into a 3-5 layered graphitic cages was observed. Lattice spacing measurement of the graphitic cage gives an interlayer distance value of 0.337 nm. This value is quite close to d002 spacing of graphite. Also, diffraction pattern of the crystalline core region consisted with the (111) plane of TiC.

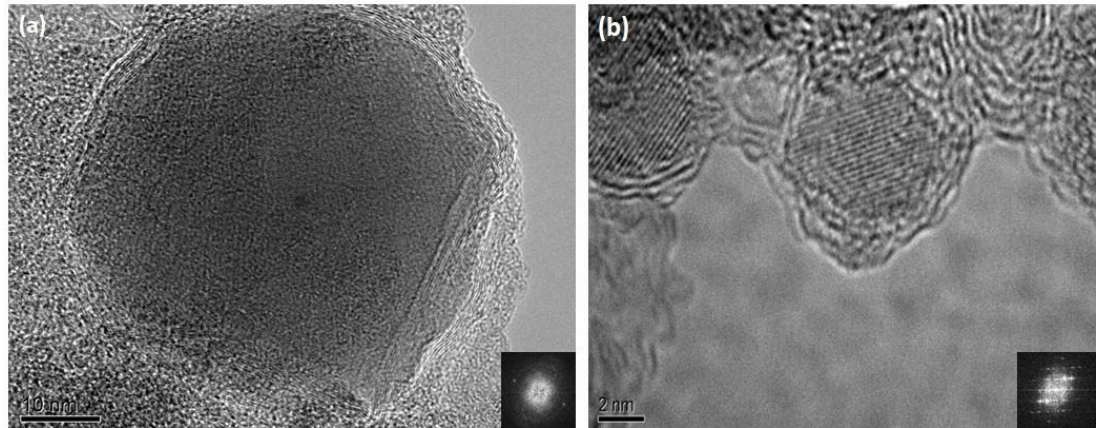


Figure 2. 9 TEM images of the distinct core shell structure obtained from the spark discharge process of a) vanadium and b) titanium electrodes. Insets shows FFT image of the core regions.

TEM images of encapsulated copper nanoparticles are given in Figure 2.10(a, b). In the outer shell, (002) planes of graphitic layers with 0.343 nm spacing was observed and in the core region, (111) plane of copper element was detected from the FFT image. The copper nanoparticle partially fills the inner space of the nanocapsule, leaving a cavity inside. TEM images of the spark discharge process of silicon elements are given in Figure 2.10(c, d). Small particles in the range from 3-5 nm were present, but the size could go up to 70 nm. TEM micrographs of a relatively large nanoparticle are given in Figure 2.10(c). Nanoparticle spherical is shape is encapsulated by shells with a varying number of layers. Encapsulating layer comprising 5 individual layers is 1.35 nm thick. This gives an interlayer distance value of 0.336 nm. This value is quite close to d002 spacing of graphite. Figure 2.10(d) shows a TEM image of another particle where the imaging at the edge of the particle. It is seen that the layered shell comprises more than one particle. This implies that the particle is an agglomerate of smaller particles. It should be noted that the lattice spacing in one of these particles matches d111 of Si.

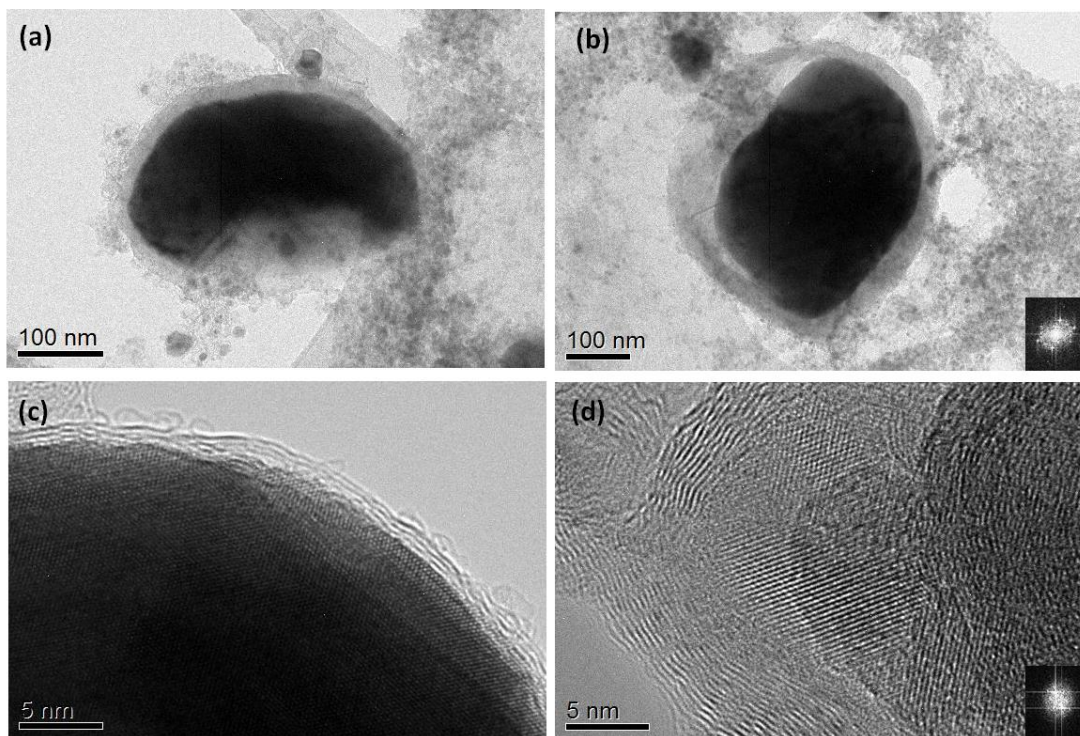


Figure 2. 10 TEM images of the a,b) partially filled copper core shell structure. c) the surface of an encapsulated particle for the silicon electrode d) silicon nanoparticle encapsulated in carbon cages. Inset shows FFT images of the core regions.

TEM image of the spark discharge process of magnesium is given in Figure 2.11. Nanoparticles were embedded in carbonaceous matrix instead of encapsulated in carbon cages. Lattice spacing measurements of magnesium nanoparticles showed that d-spacing values were consistent with the (100) and (101) plane of magnesium. Average particle size for magnesium nanoparticle is nearly 5 nm.

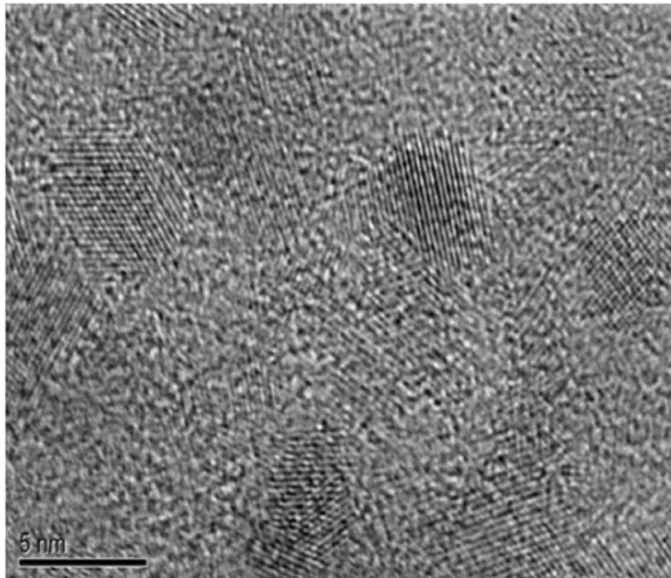


Figure 2. 11 TEM images of the nanoparticles embedded in carbonaceous matrix obtained from the spark discharge process of magnesium. Inset shows FFT images of the crystalline regions.

Observations reported above imply that it is possible to classify elements into different groups depending on their encapsulation behavior. From this point of view, elements; W, V, Ti, Si are carbide formers and FFT taken from these particles in the current study verified that they were indeed carbides. Still they were successfully encapsulated by graphitic layers. This is in contrast to a study by Seraphin *et al.* (1996) Where using arc discharge they observed no encapsulation with strong carbide forming elements. This was explained on the basis that while the nanoparticles are condensing they consume carbon in their vicinity while forming the carbides leaving no carbon for shell formation. Obviously this argument is not valid for the current case where successfully encapsulated carbides were obtained with the spark discharge. This difference in the encapsulation behavior may be attributed to the use of different synthesis methods. Arc discharge and the spark discharge with the geometries implemented in the respective studies could produce different carbon-to-element ratio in the gas phase. Additionally, the use of methane in addition to carbon electrode in the present work makes this ratio richer in C content providing source of carbon for encapsulation.

All elements that are studied in the present work were successfully encapsulated either in elemental or in carbide form. This is except for Mg where particles were

deposited onto carbonaceous matrix forming an embedded structure rather than core-shell structure. The case of Cu is intermediate since it produced a partially filled core-shell structure.

Elements used in the present study are listed in Table 2.2 in the decreasing order of their condensation temperature. Table also contains elements which had been intensively studied in the literature with respect to their encapsulation behavior. Also, included in this table are data related to the core structure whether it is elemental or in carbide form.

Data reported in Table 2.1 are shown plotted in Figure 2.12. As can be seen in the graph, elements may be divided into three groups. Those whose condensation temperature is higher than that of carbon form one of these groups. In this group, the element condenses first followed by the condensation of carbon. W is in this group, but there are also other elements such as Ta, Nb, Zr not investigated in the present work. The formation of well-defined graphitic layers in the case of W nanoparticles imply that carbon condensing onto metallic particles form regular graphitic layers, one onto the other, yielding quite a thick shell.

Many of the elements shown in Figure 2.12 have condensation temperatures that are less than that of carbon. Here it is expected that, as explained by Elliot *et al.* (1997), element condenses onto carbon clusters or form separate clusters forming a mixture. As the condensates cool down, depending on the element, they may solidify into carbide or remain in the elemental form expelling the entrapped carbon. The excess carbon whether the core is carbide or element, form encapsulating graphitic layer. It should be mentioned that the carbon entrapped within liquid metal favors the graphene formation as verified in studies conducted in a different context (Zeng *et al.* 2014).

Many of elements on the right-hand side of carbon form partially filled core-shell structure. Such elements are indicated in Figure 2.12 with partially filled symbols just below the histograms. A striking example of this, in the current work, is copper. Mechanism by which partially filled core-shell structure is formed was a subject of considerable interest (Saito *et al.* 1994, Saito 1995). Saito (1995) explained that this

was due to the entrapped carbon inside the condensate and as they are expelled and form graphitic layer leave behind an unoccupied volume. They further claimed that in such cases the shell grows from inside. Similar explanations were advanced by Seraphin *et al.* (1996) and Elliot *et al.* (1997).

Partially filled core-shell structure that is formed in copper, in the present work, contains an empty volume, roughly 1/7th of the total. In La series alloys, the empty fraction can be even higher. Based on the rough evaluation of micrographs given for La and Y by Saito (1995) yields fractions that are as high as ½, i.e. half of the volume inside the shell is empty.

Table 2. 2 Encapsulation tendency of the elements as determined from the current work supplemented by data from the literature. Elements are ordered according to their condensation temperature. Elements Ta, Nb and Zr whose condensation temperature is greater than C are also included in the table.

Elements	T <sub>cond</sub> (K)	T <sub>m</sub> (K)	Method	Encapsulation (Yes/No)	Ref.
W	5933	3683	Spark Discharge	Yes (WC)	Current Work
Ta	5698	3269			
Nb	5200	2741			
Zr	4650	2125			
C	4098				
Pr	3793	1204	Arc Discharge	Yes (PrC <sub>2</sub> )	(Saito <i>et al.</i> 1994)
La	3737	1191	Arc Discharge	Yes (LaC <sub>2</sub> )	(Saito <i>et al.</i> 1993, Saito <i>et al.</i> 1994)
Ce	3706	1071	Arc Discharge	Yes (CeC <sub>2</sub> )	(Saito <i>et al.</i> 1994)
V	3680	2163	Spark Discharge	Yes (VC)	Current Work
Lu	3675	1906	Arc Discharge	Yes (LuC <sub>2</sub> )	(Saito <i>et al.</i> 1994)

Table 2.2 (Continued)

Y	3611	1795	Arc Discharge	Yes (YC <sub>2</sub> )	(Saito <i>et al.</i> 1994)
Ti	3560	1941	Spark Discharge	Yes (TiC)	Current Work
Gd	3546	1586	Arc Discharge	Yes (GdC <sub>2</sub> )	(Saito <i>et al.</i> 1994)
Si	3538	1683	Spark Discharge	Yes (SiC)	Current Work
Tb	3503	1629	Arc Discharge	Yes (TbC <sub>2</sub> )	(Saito <i>et al.</i> 1994)
Nd	3347	1294	Arc Discharge	Yes (NdC <sub>2</sub> )	(Saito <i>et al.</i> 1994)
Co	3200	1768	Laser Ablation, Solution Plasma Processing, Arc Discharge, Carbon Arc	Yes	(Zhang <i>et al.</i> 2013, Kang <i>et al.</i> 2016, Jiao and Seraphin 1998, Seraphin <i>et al.</i> 1996, McHenry <i>et al.</i> 1994)
Ni	3186	1726	Pulsed Plasma, Solution Plasma Processing, Arc Discharge	Yes	(Jiao and Seraphin 1998, Seraphin <i>et al.</i> 1996)
Er	3141	1802	Arc Discharge	Yes (ErC <sub>2</sub> )	(Saito <i>et al.</i> 1994)

Table 2.2 (Continued)

Fe	3134	1808	Chemical Vapor Deposition, Thermal Plasma Jet, RF Thermal Plasma, Solution Plasma Processing, Arc Discharge,	Yes	(Xiaomin <i>et al.</i> 2006, Bystrzejewski <i>et al.</i> 2011, Bystrzejewski <i>et al.</i> 2009, Abdullaeva <i>et al.</i> 2013, Kang <i>et al.</i> 2016, Seraphin <i>et al.</i> 1996)
Sc	3103	1814	Arc Discharge	Yes (Sc <sub>15</sub> C <sub>19</sub> )	(Saito <i>et al.</i> 1994)
Ho	2973	1747	Arc Discharge	Yes (HoC <sub>2</sub> )	(Saito <i>et al.</i> 1994)
Cu	2840	1356	Spark Discharge	Yes	Current Work
Dy	2840	1685	Arc Discharge	Yes (DyC <sub>2</sub> )	(Saito <i>et al.</i> 1994)
Tm	2223	1818	Arc Discharge	Yes (TmC <sub>2</sub> )	(Saito <i>et al.</i> 1994)
Sm	2067	1347	Arc Discharge	No	(Saito <i>et al.</i> 1994)
Eu	1800	1095	Arc Discharge	No	(Saito <i>et al.</i> 1994)
Yb	1469	1092	Arc Discharge	No	(Saito <i>et al.</i> 1994)
Mg	1363	921	Spark Discharge	No	Current Work
			Thermal Plasma	No	(Aktekin, 2013)

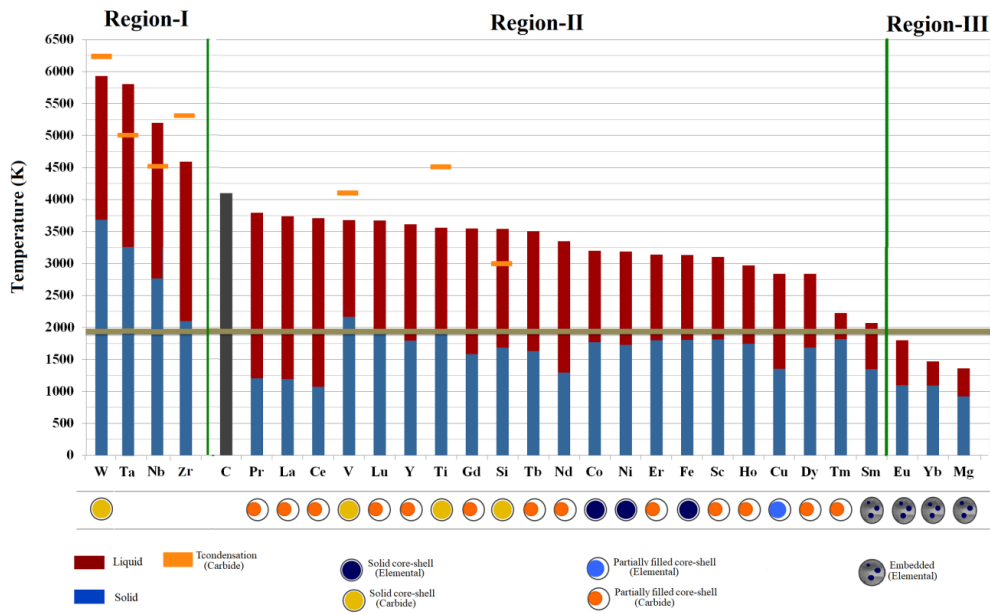


Figure 2. 12 Regions of different encapsulation behavior. Elements are ordered based on their condensation temperature. Region I yield a sound core-shell structure and cover elements/compounds whose condensation temperature is greater than that of carbon (graphite). Horizontal line drawn at 1900 K is the estimated temperature for carbon shell formation. Elements in Region II might yield sound or partially filled core-shell structure-see legends under the figure. Region III covers elements whose condensation temperature is less than 1900 K and therefore do not encapsulate but yield embedded structure.

The presence of empty volume inside the shell may well be due to expulsion of carbon from the liquid metal as proposed in Saito-Seraphin model explained by Elliot *et al.* (1997). Clearly, the shrinkage as the liquid metal cools down and then solidify could also contribute to this empty volume. Knowing the size of the shell, it is possible to calculate how much shrinkage would take place during cooling and solidification of the liquid metal provided that encapsulation temperature is known.

Carbon condenses at 4098 K. Thus it is logical to assume that carbon clusters are present in the discharges below this temperature. Precisely, when entrapped clusters are expelled from the liquid metal is not known, but it is possible to carry out a reverse calculation and determine the temperature that would be compatible with the shrinkage observed experimentally. This temperature may also be taken as the encapsulation temperature.

Equating the volume of the core-shell structure in Figure 2.10(b) yields values of  $26.5 \times 10^6 \text{ nm}^3$  and  $22.5 \times 10^6 \text{ nm}^3$  for the inner shell and the core of the solidified copper, respectively. Then, following the above approach  $26.5 \times 10^6 \text{ nm}^3$  liquid metal are wrapped by graphitic layers at the temperature of encapsulation and then cooled down to room temperature yielding  $22.5 \times 10^6 \text{ nm}^3$  copper. This implies a volume contraction of by a factor of 0.15. To obtain such shrinkage due to cooling down of the liquid and the ensuing solidification, the density of copper condensate should be less by the same factor. Considering that the density of copper at room temperature is  $8960 \text{ kg m}^{-3}$ , the required density was calculated according to the Assael et al. (2010) as a number of  $7616 \text{ kg m}^{-3}$  in the liquid state. This corresponds to a temperature of 1900 K. This is probably the temperature at which the encapsulation was taken place around the condensate.

This estimated temperature of encapsulation, 1900 K, whether this is specific to copper or applicable to all elements are not known. Assuming that this is general and applicable for condensation of all elements yield a limit for successful encapsulation. This temperature was marked in Figure 2.12 as horizontal line cutting many of the elements in condenses (solid or liquid) form. It may be stated that elements need to be in condense form, i.e. liquid or solid at around 1900 K for successful encapsulation. Elements that are still in gaseous state at around 1900 K probably will not promote encapsulation or even if they do they would not yield an acceptable amount of solid phase inside the shell.

Above arguments imply a minimum temperature for carbon encapsulation. This temperature appears to be in the neighborhood of 1900 K. In Figure 2.12, a vertical line is placed, between elements whose condensation temperature is above and below this value. Metal/compounds that are in gas phase around this temperature, i.e. in Region III in Figure 2.12, are difficult to encapsulate. In such conditions, metals/compounds would tend condense onto already condensed carbonaceous matrix. It should be mentioned Mg probably constitutes an example for this. With condensation temperature of 1363 K Mg is still in gaseous state at the encapsulation temperature of 1900 K. Thus, no core-shell structure is formed. Instead Mg condenses onto already condensed carbonaceous material forming the embedded

structure. It appears that Mg is not the only element in this category as elements such as Zn, Eu, Yb have low condensation temperatures and therefore they are likely to form embedded structure rather than the core-shell structure.

## **2.4 Conclusion**

In this chapter, encapsulation behavior of a number of elements W, V, Ti, Si, Cu and Mg were studied using a spark discharge generator. Here the element in question was made anode and used against a graphite rod forming the cathode in a chamber through which argon flow was maintained. Carbon source was further enriched by adding methane to the argon flow. Main findings of this study may be summarized as;

- Elements W, V, Ti, Si formed carbides which were encapsulated successfully by graphitic layers forming a sound core-shell structure.
- Cu could also be encapsulated but formed a partially filled core-shell structure. This was attributed to relatively low condensation temperature of Cu where considerable shrinkage seems to occur after the encapsulation.
- Mg could not be encapsulated in a core-shell structure but rather it yields a composite structure in which elements are condensed onto already condensed carbonaceous material forming an embedded structure.

Lastly, analysis of current observations coupled with those already reported data in the literature implies a simple mechanism for encapsulation. According to this, metals and compounds that are solid above the condensation temperature of carbon give rise to a sound core-shell structure. Elements whose condensation temperature is less than that of carbon could still produce a core-shell structure which may be partially filled. It is estimated that the process of graphitic encapsulation is complete around 1900 K and the formation of partially filled core-shell structure depends on the shrinkage of liquid metal upon cooling to room temperature. Based on this estimated temperature, it is concluded that elements and compounds whose

condensation temperature is below the encapsulation temperature fail to develop core-shell structure. Instead, they form embedded composite structure.



## CHAPTER 3

### INDUCTION PLASMA SYNTHESIS OF CARBON ENCAPSULATED SILICON NANOPARTICLES

#### 3.1 Introduction

<sup>2</sup>Plasma technology is advanced method to produce materials having improved functionality in current years. As a result of high temperature and reactivity of the plasma, chemical reactions encouraged.

There are several methods that are employed to produce plasmas, such as; passing current through the gas, high frequency discharge, high energy particle beam, etc. Plasma can be classified into two categories. These are “non-equilibrium” or “cold plasma” and “thermal plasma” or “hot plasma”. Non-thermal plasmas are also frequently called, “non-equilibrium” plasmas because they are characterized by a large difference in the temperature of the electrons relative to the ions and neutrals. Non equilibrium plasmas have therefore low energy density. Low power RF, microwave or DC sources can be used to create non-thermal plasmas under vacuum condition. Non equilibrium plasma can be used for such applications as plasma etching, film deposition, surface modification (Selwyn *et al.* 2001, Taylor and Pirzada 1994).

Thermal plasmas are characterized by equilibrium, between electrons, ions and neutrals in terms of temperature. Therefore, they have high energies. Direct (DC), alternating current (AC) or radio frequency (RF) or microwave sources (MF) can be used for this purpose. Thermal plasma is used in a wide variety of applications this includes coating technologies such as plasma spraying, plasma chemical vapour deposition (CVD). Another application of thermal plasma which in recent years are

---

<sup>2</sup> Data and main findings in this chapter were published with a title “Carbon Encapsulated Silicon Nanoparticles as Anodes for Lithium Ion Batteries” ECS Transactions, 77 (11) (2017) 373-382.

gaining wide acceptance is the synthesis of fine/nano powders, extractive metallurgy i.e. recovery of metal and medical waste processing (Selwyn *et al.* 2001, Taylor and Pirzada 1994).

Thermal plasma torches are mainly of two types; DC and RF. In the RF induction plasma torches, energy to plasma is accomplished by the electromagnetic field. For this reason, contamination is not a problem. Another advantage of this torch design is the operation of plasma torches in a wide range of operating conditions including inert, reducing, oxidizing and other atmospheres. General choice for the plasma gas is usually pure argon or mixture of it with other gases. Central plasma gas, Argon, used to start and sustain the plasma. Also air, helium, oxygen or mostly hydrogen is used to contribute the plasma forming. In addition to the plasma forming gases, injection of powder gas, also known as carrier gas, is responsible from the introduction to the material to the plasma region. Also, temperature and flow field during a discharge process shows that large volume of plasma is observed for the RF induction plasma systems. Also, in addition to the large plasma volume, long residence time of the particles, in the range of 10-20 m<sup>s</sup>, is another typical character of RF induction plasma reactors (Boulos 1991, Gomez *et al.* 2009).

Thermal plasma technologies offer a versatile, cost effective technology for the wide range of possible applications. High temperature formation (5000 K), pure and controlled atmosphere, high throughput with compact reactor geometry, high quench rates (10<sup>6</sup> K/s) and low gas flow rate are the main characteristics of the thermal plasma systems. In addition to this, plasma processing has several advantages especially in the field of nano material production (Samal *et al.* 2010, Taylor and Pirzada 1994).

Among the thermal plasma process, RF inductively coupled thermal plasma process is generally used to synthesize the nanopowders as mentioned in above. High temperature in the plasma region that resulted with chemically reactive species formed in the plasma through vapor phase reaction and rapid quench rate that lead to production of spherical and ultrafine particles are the main advantages of this technique to produce nanosized materials. Also, short and controllable residence

time in the high temperature zone is another advantage of this process. Precursors, usually in the form of powder are fed into the plasma reactors. Also, atmosphere conditions include inert, oxidizing and reducing in the plasma region can be adjustable (Gomez *et al.* 2009). Due to all of these properties, RF inductively coupled thermal plasma process plays a crucial role in the nanoparticle synthesis. In Figure 3.1 shows the general design of the plasma reactor system used to produce nanoparticle.

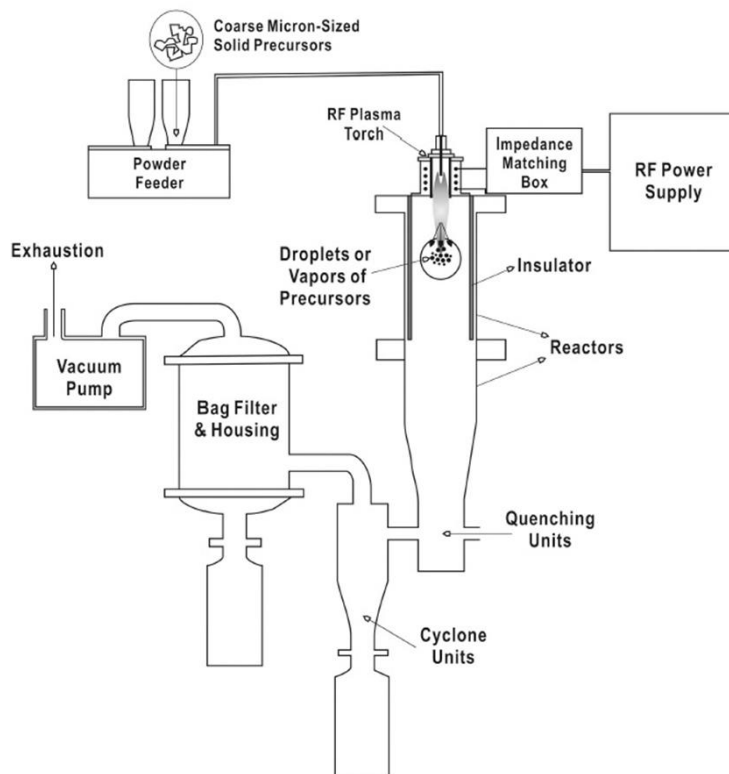


Figure 3. 1 A Schematic of an RF Plasma Torch System Designed for Synthesis of Nano-sized Powders (Seo and Hong 2012).

In literature, RF induction thermal plasma systems used to produce nanopowder of good quality with a particle size of less than 100 nm are applied for a wide range of material. The range of possible product covers a metals, ceramics, glasses, carbonaceous materials and other functional composites like metal oxide catalyst and core-structure nano materials (Seo and Hong 2012).

As it is well known fact that many interesting properties includes optical, electrical etc. have been found in metal particles with sizes of <50 nm. Due to their advantages includes high temperature region, high purity, RF plasma torches have been widely used to produce variety of nano sized metal powders in the form of element and alloy. For example, Al, Ni, W, Fe, Ni and Cu are the well-known examples in this area (Seo and Hong 2012). In addition to the metals, especially, in recent years numerous carbon materials such as fullerenes (Todorovic-Marković *et al.* 2003), carbon nanotubes (Kim *et al.* 2009) and graphene (Zhang *et al.* 2015) have been synthesized through this technique with a great success. A few examples from the synthesis of metals and carbon materials by RF induction thermal plasma method will give below.

Nam *et al.* (2013) have investigated the synthesis of nano-sized Ni powder by RF thermal plasma process of Ni metal. This study revealed that RF thermal plasma method is a simple and efficient treatment to produce nano-sized Ni metal powders from the micro-sized Ni metals.

Aktekin *et al.* (2014) have studied the RF thermal plasma synthesis of Mg<sub>2</sub>Ni nanoparticles. For this purpose, two injection probes position was used in the reactor and powders were fed into the system in elemental and pre-alloyed form. According to the result, feeding of powders in the elemental form is a more logical approach to produce Mg<sub>2</sub>Ni because feeding process of pre-alloyed Mg<sub>2</sub>Ni powders resulted with the formation of two different phases.

Kim *et al.* (2009) have reported the characterization and purification process of single-walled carbon nanotubes (SWNTs) synthesized by induction thermal plasma process. TEM image of the purified products showed that synthesis of SWNTs with a 10-20 nm sized range was successful. This study revealed that induction thermal plasma method is a useful method for the synthesis of high amount of pure SWNTs when integrated with proper purification treatment.

Zhang *et al.* (2015) investigated the large scale synthesis of few layer graphene by RF induction thermal plasma process using methane gas as a carbon source. Direct conversion of the CH<sub>4</sub> to few layer graphene was resulted with synthesis of 5-layer

graphene sheets in a 200-500 nm sized range. Also, this study showed that H<sub>2</sub> atmosphere in the process is a key factor to convert the nanosphere structure form of carbon to nanosheet.

A number of other processes involving plasma chemical synthesis have also been developed for the synthesis of high purity ceramic materials in nanosized. These can be grouped, depending on the chemical nature of the produced powders. Some of the examples from the applications are given here.

Oxides: Al<sub>2</sub>O<sub>3</sub>, SiO<sub>2</sub>, MgO, TiO<sub>2</sub>

Carbides: SiC, TiC, B<sub>4</sub>C, WC

Nitrides: Si<sub>3</sub>N<sub>4</sub>, AlN, TiN, BN (Boulos 1991)

Oh *et al.* (2005) have reported the synthesis of titanium dioxide (TiO<sub>2</sub>) nanopowders from the oxidation process of titanium nitride (TiN) using radio frequency (RF) induction thermal plasma. HRTEM images of TiO<sub>2</sub> fine particles synthesized with mixed plasma showed that nanoparticles appeared in the form of polyhedrons and size of particles was 50 nm.

Guo *et al.* (1995) synthesized the ultrafine high purity SiC powder from the silicon powder and methane gas using induction plasma reactor. XRD studies showed that collected powders includes different phases which are high amount of silicon carbide, unevaporated elemental silicon, free silicon and free carbon.

In addition to the metals, carbon materials and ceramics such as, oxides, carbides and nitrides, synthesise of the other functional composite materials includes supported metal catalysts and core-shell structured nano-powders by RF thermal plasma have been studied. Among them, core shell structure materials have a special interest due to promising properties. Especially, thermal plasma treatment of mixture of carbonaceous materials and metal powders and creation of carbon cage and metal core structure has a special interest for the magnetic materials includes Fe, Co, Ni etc. (Seo and Hong 2012). A few examples from the recent applications, especially in the core shell structures, of the RF plasma torches will be given.

Bystrzejewski *et al.* (2009) produced carbon encapsulated Fe, Fe<sub>3</sub>N and NdC<sub>2</sub> nanoparticles via RF thermal plasma process. Electron microscopy showed that core shell structure in a 10-30 nm core diameter was successfully synthesis. Carbon coating contained defect in the structure with a changing crystallization tendency. Also, study showed that methane can be useful choice if high degree of crystallinity and low amount of excess carbon in the matrix wanted.

Cheng *et al.* (2013) have reported the titanium boride-boride core-shell nanoparticles were synthesized by the RF thermal plasma process. Successful RF thermal plasma synthesis of this complex structure has significant attention because high melting and boiling of precursor is a considering factor for other production techniques.

In this context, Thermal plasma processing of silicon materials has been studied recently due to superior properties especially as anode materials. High gravimetric (4200 mA h g<sup>-1</sup>) and volumetric capacity (2400 mA h cm<sup>-3</sup>) of silicon anodes leads to replacement of these materials with graphite in Li- ion batteries (Choi *et al.* 2012). The discharging potential of Si with respect to Li/Li<sup>+</sup>, is lower than most of other alloy type and metal oxide anodes. Such a low operation potential can lead to a high energy density. Furthermore, silicon is environmentally friendly, cheap and abundant element. (Ashuri *et al.* 2016, Su *et al.* 2013).

However, there are several challenges associated with the use of bulk Si anode materials. Silicon suffers from significant volume expansion, ~300%, during lithium insertion and extraction. The resulting stress leads to the electrode pulverization which may destroy the conductive network between the active material and the current collector. It leads to decrease in the cyclic performance of the battery. Also, deformation causes stress, fracture; change in morphology of electrodes, in Figure 3.2(a) (Rahman *et al.* 2016). Also, reformation of the SEI leads to more thicker SEI formation, see in Figure 3.2(b). Another challenge is the low conductivity of Li<sup>+</sup> in Si (Zuo *et al.* 2017). These results lead to decay in battery capacity after the first few cycles.

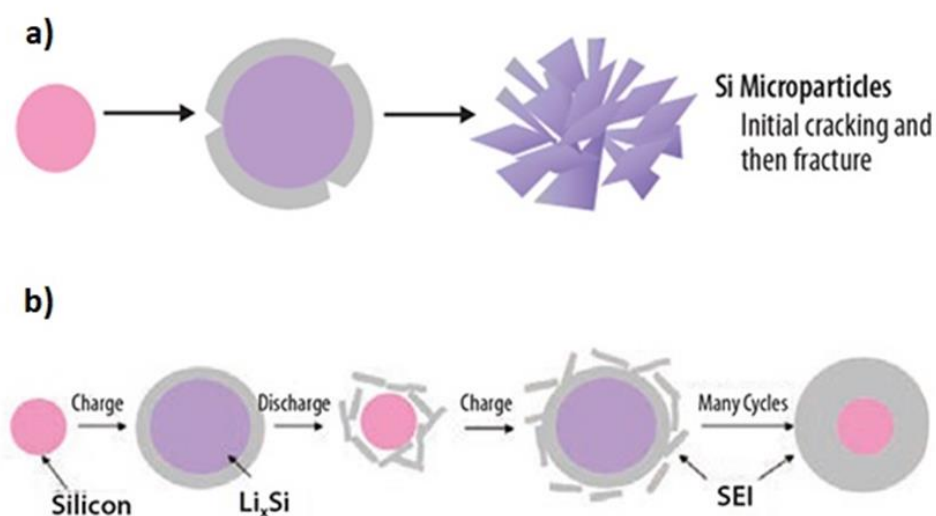


Figure 3. 2 a) Schematic of failure mechanism of Si electrode. b) Schematic of SEI formation on a pure silicon surface during charge/discharge cycles (Rahman *et al.* 2016).

Tremendous efforts have been made to improve the performance of Si anode. To address these issues, several strategies were employed including utilization of nanoscale silicon, compositing with stress relief buffer, and constructing physical compartment to accommodate volume expansion (Zuo *et al.* 2017).

Among them, formation of the physical compartment to adjust the volume expansion is the most preferred one. It includes construction of core-shell, yolk-shell and hollow core-shell structures (Zuo *et al.* 2017).

Among them, carbon encapsulation of silicon nanoparticles is of special interest because of their use as anodes in lithium ion battery. Synthesis of core-shell, yolk-shell or hollow-shell structures have been carried out for the silicon anode materials (Hwa *et al.* 2012, Zhang *et al.* 2006, Liu *et al.* 2012 and Li *et al.* 2012). These studies generally focus on solution based methods, but in this section we will review encapsulation of silicon nanoparticles via a gas-phase route, i.e. Carbon arc process and thermal plasma.

Seraphin *et al.* (1996) have used graphite electrodes of which the anode drilled to add SiO<sub>2</sub> particles in a helium atmosphere. In this experiment SiO<sub>2</sub> was converted to SiC.

Chaukulkar *et al.* (2014) have used nonthermal, radio frequency (RF) plasma to synthesize carbon coated crystalline silicon nanoparticles. The RF plasma system was operated under 50 W powers in the  $\text{SiH}_4$  with Argon gas. In the system,  $\text{C}_2\text{H}_2$  was used as a carbon source, Figure 3.3. Silicon nanoparticles obtained in this work were encapsulated with amorphous carbon. Moreover, XPS and TEM characterization showed the formation of thin and cubic  $\text{SiC}$  layers between the core and shell. They concluded that process has to be changed to obtain low ratio of  $\text{SiC}$  formation.

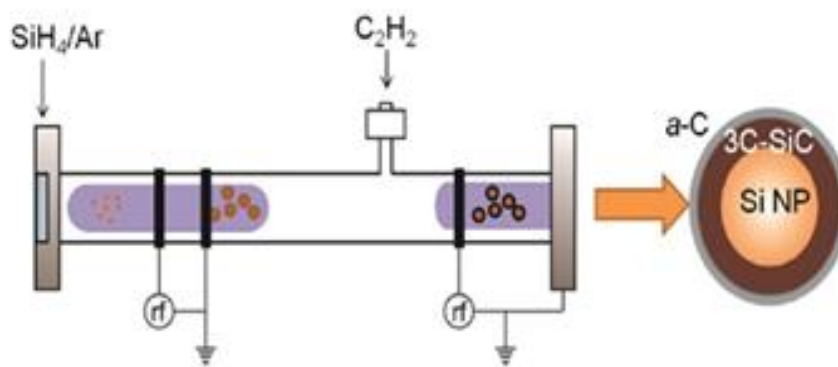


Figure 3. 3 Schematic of the tubular reactor equipped with two radio frequencies, capacitive-coupled plasma sources used to synthesize carbon-coated silicon nanoparticles (Chaukulkar *et al.* 2014).

Guo *et al.* (1995) used induction thermal plasma with elemental silicon and methane to synthesize carbon encapsulated particles. Methane and elemental silicon powder were used as precursor. In 40-80 nm sized range nanoparticles were synthesized in the form of combined phases includes Si,  $\text{SiC}$ , low ratio of free silicon and free carbon. They observed no encapsulation in this study. Study revealed that reaction path in the plasma system is based on the evaporation of the pure silicon and carburization process of formed vapor with methane gas.

Lee *et al.* (2016) have reported that thermal plasma synthesis of  $\text{Si}/\text{SiC}$  nanoparticles from silicon and activated carbon powders. XRD, SEM and TEM were used to characterize the produced powders. Plasma processing resulted with the synthesis of nanosized  $\text{Si}/\text{SiC}$  nanocomposite in a 20-60 nm sized range, where elemental silicon (15 nm) was formed on the surface of  $\text{SiC}$ .

L1 and Ishigaki (2007) have shown that core shell structure of Si and SiC formed from silicon carbide shell and silicon core were synthesized by thermal plasma in a Ar-H<sub>2</sub>-CH<sub>4</sub> atmosphere. TEM studies showed that a uniform distribution of SiC nanoparticles with a 50-150 nm sized and long SiC nanotubes were formed in Si matrix. They suggested that it resulted from the diffusion of Si to the outer structure and the growing of SiC towards through Si droplets.

In this chapter, encapsulation of silicon nanoparticles into the carbon cages was carried out RF induction. This involved use of the Si powder and methane as a carbon source. Two precursor geometries were investigated; co-feeding of Si and methane and post feeding of methane and after Si particle formation. Also, effect of plasma parameters includes, feeding geometry of the starting powders and methane gas flow rate were investigated.

## **3.2 Experimental**

### **3.2.1 RF Plasma System**

In this work, RF induction thermal plasma system (Tekna Plasma Systems Inc.) was used to synthesize the carbon encapsulated silicon nanoparticles. A schematic drawing of the complete RF thermal plasma system is given in Figure 3.4. The system consists of an RF generator (30 Kw, 2- 5 MHz nominal frequency), a plasma torch, a gas delivery system, a precursor feeding system, a quenching chamber and powder collecting system the vacuum unit.

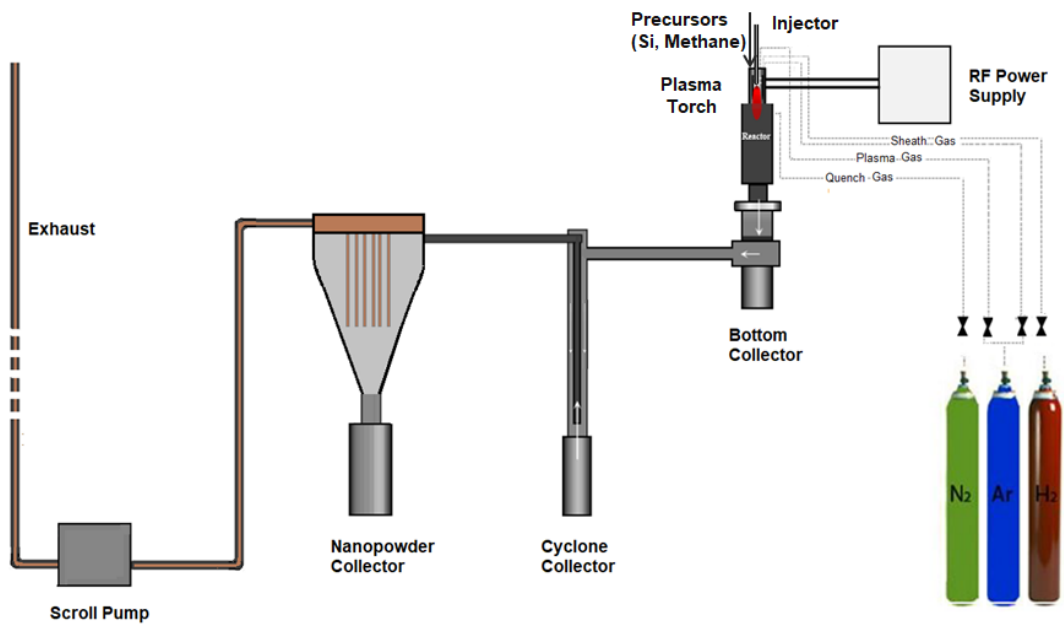


Figure 3. 4 Schematic design of RF induction thermal plasma system (Aktekin *et al.* 2014). Collection of produced powders is done from the 3 collection unit of the plasma system, namely bottom collector, cyclone collector and powder collector (seen in Figure 3.5). Division in the size range of the produced powders done by aerosol flow of the collection units of the plasma system. Large particles and relatively small particles ( $> 1-2 \mu\text{m}$ ) are collected from the bottom collector and cyclone collector. On the other hand, powders collected from the powder collector are a nano sized range.



Figure 3. 5 a) Actual design of the bottom collector, cyclone collector, powder collector, respectively. Actual view from the collection unit of the b) bottom collector c) cyclone collector d) powder collector.

### 3.2.2 Plasma Reactor

A schematic drawing of an RF plasma torch is given in Figure 3.6. The torch consist of two sections; the central portion where the plasma is formed and the outer portion where sheath gas is maintained. Plasma gas is argon flowing in within the plasma confinement tube. Sheath gas is a mixture of argon and hydrogen maintained between the plasma confinement tube and the torch wall.

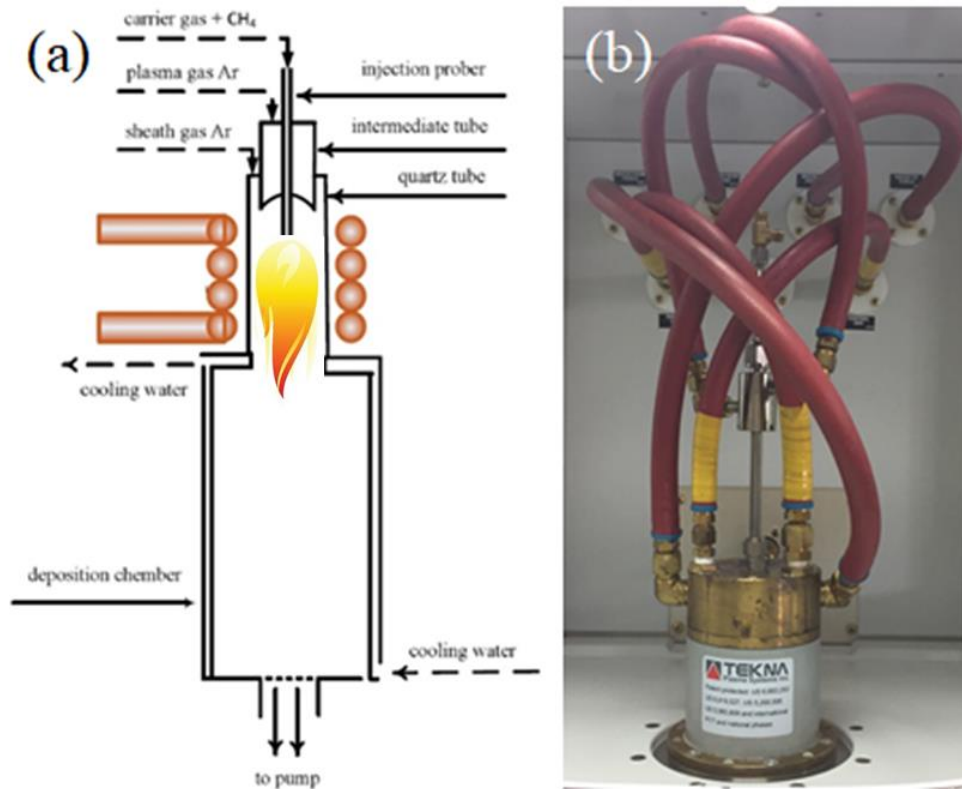


Figure 3. 6 a) Schematic diagram of the RF induction thermal plasma system. b) Photograph of the plasma torch.

To synthesize encapsulated silicon nanoparticles, silicon and methane fed into the plasma reactor via a stainless steel injector placed vertically into the torch. Silicon (Beijing Haoyun Industry, 99.99% purity, -325 mesh size) was fed in a 2.5 g/min flow rate with a vibratory powder feeding. System using Ar (Linde, 99.995% purity) as a carrier gas with a 15 slpm flow rate. Methane (99.5% purity) which was co-fed to the injector with a 1slpm flow rate was mixed with the carrier gas, Ar with 5 slpm flow rate.

All experiment was conducted at 0.97 bar (absolute) pressure i.e. the pressure was slightly less than the atmospheric. During our experiments, 25 Kw plate power was supplied to the plasma system from the induction plasma torch. The system was operated for approximately 15 minutes and powders were collected from the powder collector to structural characterization. Parameters used in the operation of thermal plasma are reported in Table 3.1.

Table 3. 1 Experimental parameters of the RF thermal plasma pyrolysis process of methane.

Parameters	Values
Plasma power/ Kw	25
Plasma gas (Ar)/slpm	15
Sheath gas (Ar /H <sub>2</sub> )/slpm	60/6
Carrier gas (Ar)/slpm	5
Process atmosphere/atm	0.97
Process duration/ min	15
CH <sub>4</sub> feeding rate/srpm	1

The system was operated for approximately 15 minutes and powders were collected from the powder collector to structural and electrochemical characterization.

### 3.2.3 Material Characterization

Nanoparticles produced via induction thermal plasma was examined with Field Emission Transmission Electron Microscope (Jeol JEM2100F). For this purpose, a small amount of powder was added to ethanol and ultra-sonicated for 5 minutes. Then a small droplet was applied with a pipet to holy carbon grid. FFT images were examined to determine d-spacing of the nanoparticles. Raman spectra were obtained for the coated samples (Renishaw inVia) at the wavelength of 532 nm. X-ray diffraction patterns were obtained (Rigaku DMAX 2200 (Cu-K $\alpha$ )) with Rietveld analysed using Maud software (Lutterotti 2011). Also, Quantachrome Corporation Autosorb-6 BET analysis instrument was used to determine the specific surface area of collected particles.

### 3.3 Results& Discussion

Silicon powder was fed with a rate of 2.5 g/min together with methane with 1 l/m. The system was operated for 15 minutes yielding an adequate amount of powders for

structural characterization. X-ray diffraction (XRD) pattern of powder produced by thermal plasma is given in Figure 3.7. Here the Rietveld refined pattern shows a multiphase material. The phases present are Si, SiC and graphite with the weight fractions of 68.6, 28.7 and 2.7 wt.% in the respective order. The refinement yields particle sizes of 101.4 nm for silicon and 63.05 nm for silicon carbide.

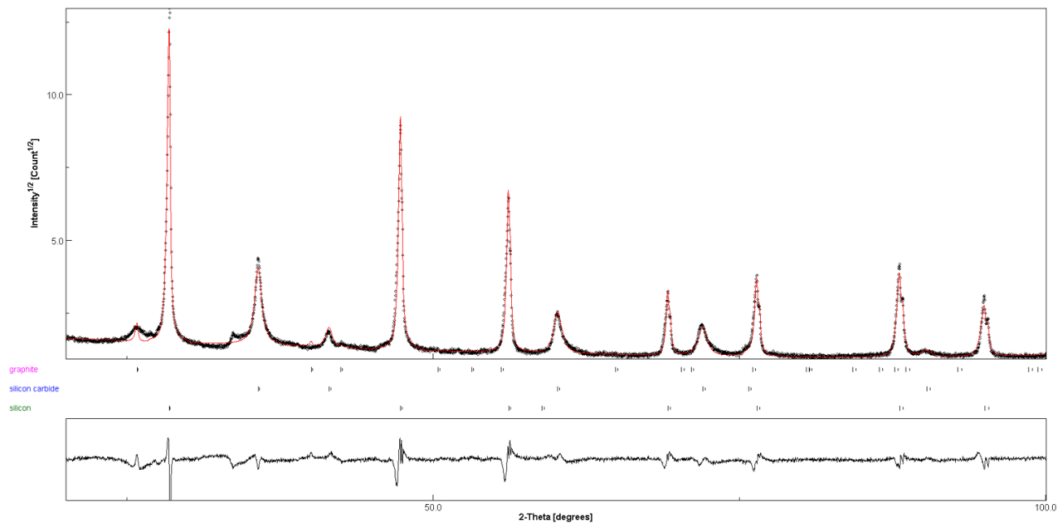


Figure 3. 7 Rietveld refinement of the X-ray diffractogram of powder synthesized by induction thermal plasma.

A typical Raman spectrum recorded from the powders is shown in Figure 3.8. The spectra show a prominent peak at  $515\text{ cm}^{-1}$  and two broad peaks at  $294$  and  $965\text{ cm}^{-1}$ . These positions are consistent with silicon, though slightly displaced as a result of small particles size. Peaks of SiC are also present but quite broad and weak in intensity as would be expected. Three peak positions at  $1347$ ,  $1577$  and  $1627\text{ cm}^{-1}$ , corresponds to carbon nanomaterials. The intensity ratio of the first two peaks, i.e. D band over G band is the measure of the disorder of the graphitic material (Bystrzejewski *et al.* 2009). This ratio has a value of 0.31, implying a high degree of crystallinity in the present case.

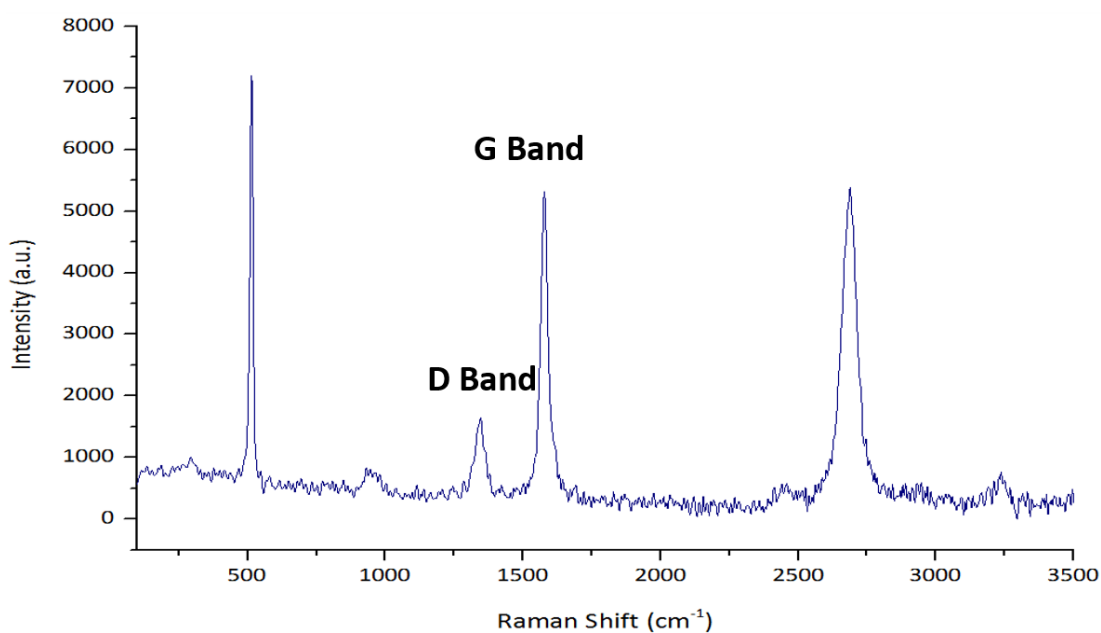


Figure 3. 8 Raman spectra of samples obtained by induction thermal plasma process.

General TEM images of powder obtain with thermal plasma are given in Figure 3.9. Here the general structure is that graphite with spherical nanoparticles. Examples of typical nanoparticles encountered in TEM examination are given in Figure 3.9(a). The images display relatively large nanoparticles. The average size evaluated for a total of 20 particles is 82 nm. Figure 3.9(b) shows a range of structures. Here in addition to the core shell structure, hollow carbon cages observed in the structure.

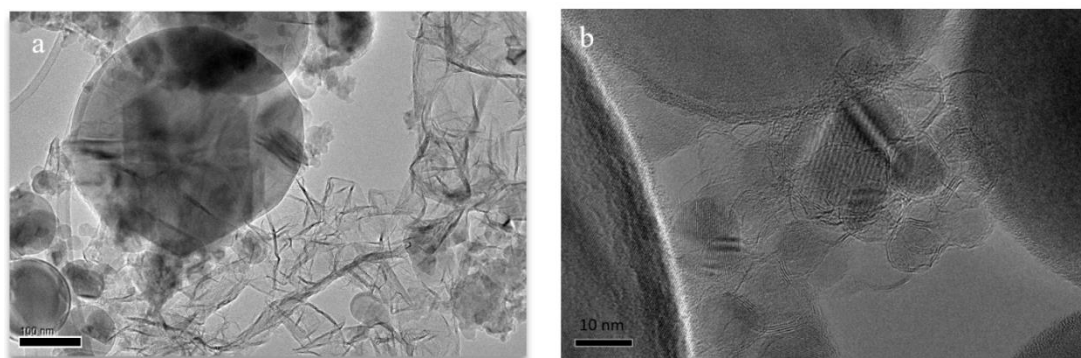


Figure 3. 9 a) Low magnification TEM images of the nanoparticles and carbon nanostructures. b) Low magnification TEM images of the core/shell structure.

Figure 3.10 shows a HRTEM image of the outer carbon layers of an edge of a nanoparticle. There are 20 and 25 carbon layers with a total thickness of 7-10 nm, which contact with the nanoparticle. The interlayer distance of approximately 0.342 nm is little larger than (002) planes of graphite crystals. Also, Figure 3.11 shows examples of nanoparticles in the synthesized powders. As shown in Figure 3.11, FFT image indicated that lattice fringe separation inside the core yielded a (101) plane of Si. Also, the particle appears to be bare where the surface is well defined probably with a thin SiO<sub>2</sub> layer.

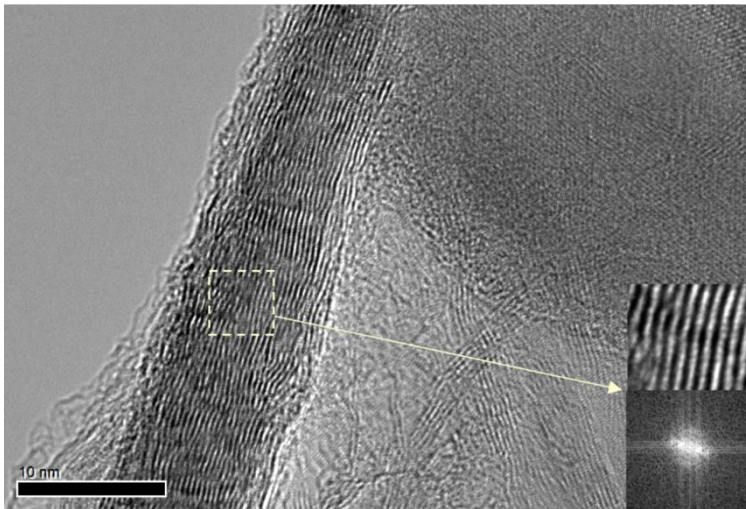


Figure 3. 10 High-resolution TEM image of the graphitic shell, showing a layered structure. Inset is the FFT image.

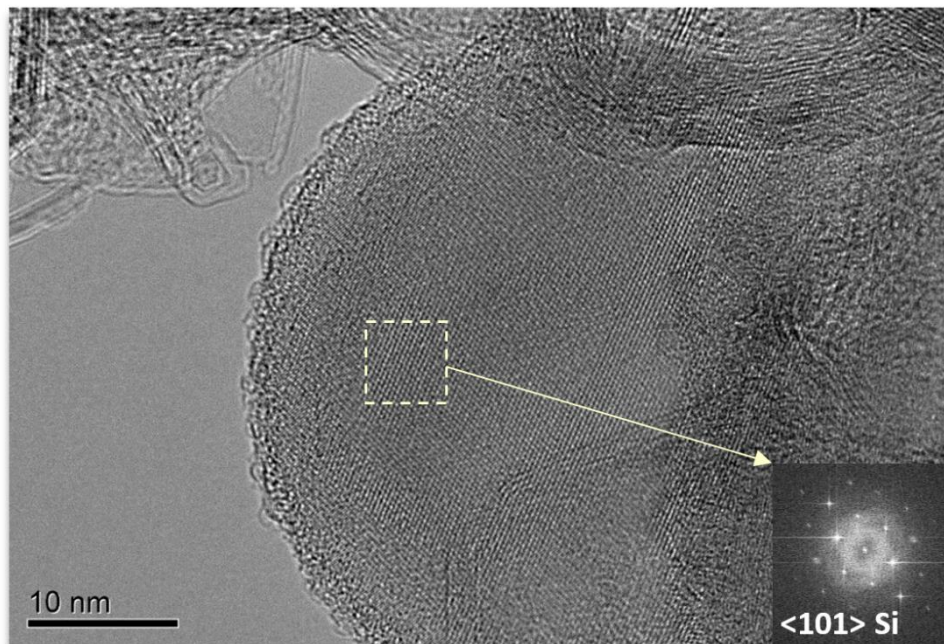


Figure 3. 11 HRTEM image of the interface between nanoparticle and carbon cage. Insets show a close-up image from the carbon cage and its FFT image.

Even though with HR-TEM examination yields a variety of structure, it is useful to emphasize that the powder produced with thermal plasma is a multiphase material where nearly two thirds of it is silicon and the rest is SiC plus a small amount of graphite.

The rapid decay in the discharge capacity given by Miser (2017) with cycling implies that the degree of encapsulation achieved in this work was not enough to provide the required stability for silicon nanoparticles in the entire structure. It is well known that size of silicon nanoparticles is a critical parameter for improved electrochemical performance. Kim *et.al* (2010) revealed that nanoscale Si particles (< 20 nm) are needed to obtain high specific capacities and good capacity retention over cycles without particle cracking. Even though some particles in the current work are in the required range, there is a considerable fraction of materials that are outside this range. Of course, in addition to size consideration, an additional problem in the current method is the formation of SiC which reduces the active ingredient in the resulting powder. The reduction in the particle size is possible and can be achieved by proper adjustment of thermal plasma parameters, the most influential of which is the rate of quench gas. By doubling or tripling the rate of quench gas,

considerable reduction can be achieved in the particle size. Also, the elimination of SiC is more difficult and probably not possible when the precursors are fed together into the reactor. This requires that encapsulated silicon particles could be achieved by post processing of pure Si nanoparticles.

### **3.4 Conclusion**

In the present chapter, an investigation was carried out for carbon encapsulation of silicon nanoparticles using thermal plasma synthesis. The following conclusions can be drawn from the present work. Thermal plasma could yield nanoparticles in useful quantities, but particle size was not sufficiently small. This could be remedied by suitable adjustments in thermal plasma parameters. It appears that Si and methane when co-fed into plasma torch, the formation of SiC is unavoidable which reduces the active ingredient in the resulting powder. Therefore, it is necessary to adopt a different methodology; Si nano powders may be produced with thermal plasma which may then be post processed for encapsulation.

## CHAPTER 4

### GENERAL CONCLUSIONS

In the present work, an investigation was carried out on carbon encapsulation of elements covering W, V, Ti, Si, Cu and Mg with special emphasis on Si. The study is made up of two parts.

In the first part, the encapsulation was achieved via spark discharge using an elemental rod against a carbon electrode, used as carbon source, under a constant argon flow. The source of carbon was further enriched by methane which was co-fed with argon into the reaction chamber. The followings can be concluded from this study;

i. Spark discharge process of elements W, V, Ti and Si were converted into carbide and were encapsulated successfully by graphitic layers producing sound core-shell structure. The elements Cu and Mg remained in elemental form, Cu yielding a partially filled core-shell structure. Mg yielded altogether different structure where Mg particles were embedded in graphitic matrix.

ii. Simple calculation based on partially filled Cu core-shell structure imply that encapsulation takes place at temperature around 1900 K. This temperature coupled with condensation temperature of graphite (4000 K) allows elements to be divided into three categories.

- Elements/carbides with condensation temperature higher than 4000 K produce a sound core-shell structure. Thus elements W, V and Ti belong to this category.

- Elements/carbides whose condensation temperature is between 4000 K and 1900 K yield sound or partially filled core-shell structure depending on the volume shrinkage during solidification.

- Elements/compounds whose condensation temperature is below 1900 K fail to develop core-shell structure. Instead, they form embedded composite structure where particles are embedded into a graphitic matrix.

In the second part, thermal plasma was used to synthesize carbon encapsulated silicon nanoparticles. Feeding Si powders together with methane into a 25 kW RF reactor yielded nanopowders which comprised SiC, Si, and graphite.

iii. SiC@C could be produced by adjusting the parameters related to plasma and feed rate of precursors it might be possible to eliminate the other constituents and obtain SiC@C nanoparticles, i.e carbon encapsulated SiC.

It may also be mentioned that there is considerable interest in developing Si@C. The current work shows that it is difficult to produce Si@C because Si is strong carbide former. For the production of Si@C, two-step process may be used; first to produce Si nanoparticles and encapsulating them by post feeding of methane at lower temperature.

## REFERENCES

Aktekin, B. (2013). Induction plasma synthesis of Mg-Ni nanoparticles. (Master's thesis). Retrieved from METU Theses Collection. (Accession No. 2550702031300926)

Aktekin, B., Çakmak, G., & Öztürk, T. (2014). Induction thermal plasma synthesis of Mg<sub>2</sub>Ni nanoparticles. *International Journal of Hydrogen Energy*, 39(18), 9859-9864.

Anastasopol, A., Pfeiffer, T. V., Middelkoop, J., Lafont, U., Canales- Perez, R. J., Schmidt-Ott, A. (2013). Reduced enthalpy of metal hydride formation for Mg-Ti nanocomposites produced by spark discharge generation, *JACS*, 135, 7891–7900.

Ashuri, M., He, Q., & Shaw, L. L. (2016). Silicon as a potential anode material for Li-ion batteries: Where size, geometry and structure matter. *Nanoscale*, 8(1), 74-103.

Athanassiou, E. K., Grass, R. N., & Stark, W. J. (2006). Large-scale production of carbon-coated copper nanoparticles for sensor applications. *Nanotechnology*, 17(6), 1668-1673.

Blomberg, S., Gustafson, J., Martin, N. M., Messing, M. E., Deppert, K., Liu, Z. (2013). Generation and oxidation of aerosol deposited Pd Ag nanoparticles. *Surf. Sci.* 616, 186–191.

Blomberg, S., Westerström, R., Martin, N. M., Lundgren, E., Andersen, J. N., Messing, M. E. (2014). A high pressure X-ray photoelectron spectroscopy study of oxidation and reduction of Rh(100) and Rh nanoparticles. *Surf. Sci.* 628, 153–158.

Boulos, M. (1991). Thermal plasma processing. *IEEE Transactions on Plasma Science*, 19(6), 1078-1089.

Byeon, J. H., Park, J. H., and Hwang, J. H. (2008). Spark generation of monometallic and bimetallic aerosol nanoparticles. *J. Aerosol Sci.* 39, 888–896.

Bystrzejewski, M., Karoly, Z., Szepvolgyi, J., Kaszuwara, W., Huczko, A., & Lange, H. (2009). Continuous synthesis of carbon-encapsulated magnetic nanoparticles with a minimum production of amorphous carbon. *Carbon*, 47(8), 2040-2048.

Bystrzejewski, M., Károly, Z., Szépvölgyi, J., Huczko, A., & Lange, H. (2011). Continuous synthesis of controlled size carbon-encapsulated iron nanoparticles. *Materials Research Bulletin*, 46(12), 2408-2417.

Chaitoglou, S., Sanaee, M. R., Aguiló-Aguayo, N., & Bertran, E. (2014). Arc-Discharge Synthesis of Iron Encapsulated in Carbon Nanoparticles for Biomedical Applications. *Journal of Nanomaterials*, 2014, 1-8.

Chaukulkar, R. P., Peuter, K. D., Stradins, P., Pylypenko, S., Bell, J. P., Yang, Y., & Agarwal, S. (2014). Single-Step Plasma Synthesis of Carbon-Coated Silicon Nanoparticles. *ACS Applied Materials & Interfaces*, 6(21), 19026-19034.

Cheng, Y., Choi, S., & Watanabe, T. (2013). Synthesis of Niobium Boride Nanoparticle by RF Thermal Plasma. *Journal of Physics: Conference Series*, 441, 012031.

Choi, N., Chen, Z., Freunberger, S. A., Ji, X., Sun, Y., Amine, K., Bruce, P. G. (2012). Challenges Facing Lithium Batteries and Electrical Double-Layer Capacitors. *Angewandte Chemie International Edition*, 51(40), 9994-10024.

Cole, J. J., Lin, E., Barry, C. R., & Jacobs, H. O. (2009). Continuous nanoparticle generation and assembly by atmospheric pressure arc discharge. *Applied Physics Letters*, 95(11), 113101.

Conte, M., Prosini, P. P., & Passerini, S. (2004). Overview of Energy/Hydrogen Storage: State-of-the-Art of the Technologies and Prospects for Nanomaterials. *ChemInform*, 35(26).

Dravid, V. P., Host, J. J., Teng, M. H., Hwang, B. E., Johnson, D. L., Mason, T. O., & Weertman, J. R. (1995). Controlled-size nanocapsules. *Nature*, 374(6523), 602-602.

Elliott, B. R., Host, J. J., Dravid, V. P., Teng, M. H., & Hwang, J. (1997). A descriptive model linking possible formation mechanisms for graphite-encapsulated nanocrystals to processing parameters. *Journal of Materials Research*, 12(12), 3328-3344.

Evans, D. E., Harrison, R. M., and Ayres, J. G. (2003). The Generation and characterization of metallic and mixed element aerosols for human challenge studies. *Aerosol Sci. Tech.* 379, 75–987.

Fu, Q., Wagner, T., Olliges, S., & Carstanjen, H. (2005). Metal–Oxide Interfacial Reactions: Encapsulation of Pd on TiO<sub>2</sub>(110). *The Journal of Physical Chemistry B*, 109(2), 944-951.

Gomez, E., Rani, D. A., Cheeseman, C., Deegan, D., Wise, M., & Boccaccini, A. (2009). Thermal plasma technology for the treatment of wastes: A critical review. *Journal of Hazardous Materials*, 161(2-3), 614-626.

Guerret-Piécourt, C., Bouar, Y. L., Lolseau, A., & Pascard, H. (1994). Relation between metal electronic structure and morphology of metal compounds inside carbon nanotubes. *Nature*, 372(6508), 761-765.

Guo, J. Y., Gitzhofer, F., & Boulos, M. I. (1995). Induction plasma synthesis of ultrafine SiC powders from silicon and CH<sub>4</sub>. *Journal of Materials Science*, 30(22), 5589-5599.

Guo, X., Wagner, M., Gutsche, A., Meyer, J., Seipenbusch, M., and Nirschl, H. (2015). Laboratory SWAXS combined with a low-pressure impactor for quasi-online analysis of nanoparticles generated by spark discharge. *J. Aerosol. Sci.* 85, 17–29.

Hwa, Y., Kim, W., Hong, S., & Sohn, H. (2012). High capacity and rate capability of core–shell structured nano-Si/C anode for Li-ion batteries.

*Electrochimica Acta*, 71, 201-205.

Jiao, J., & Seraphin, S. (1998). Carbon encapsulated nanoparticles of Ni, Co, Cu, and Ti. *Journal of Applied Physics*, 83(5), 2442-2448.

Kim, H., Seo, M., Park, M., & Cho, J. (2010). A Critical Size of Silicon Nano-Anodes for Lithium Rechargeable Batteries. *Angewandte Chemie*, 122(12), 2192-2195.

Kim, J. T., and Chang, J. S. (2005). Generation of metal oxide aerosol particles by a pulsed spark discharge technique. *J. Electrostatics* 63, 911–916.

Kim, K. S., Imris, M., Shahverdi, A., Alinejad, Y., & Soucy, G. (2009). Single-Walled Carbon Nanotubes Prepared by Large-Scale Induction Thermal Plasma Process: Synthesis, Characterization, and Purification. *The Journal of Physical Chemistry C*, 113(11), 4340-4348.

Krätschmer, W., Lamb, L. D., Fostiropoulos, K., & Huffman, D. R. (1990). Solid C<sub>60</sub>: A new form of carbon. *Nature*, 347(6291), 354-358.

Kreyling, W. G., Biswas, P., Messing, M. E., Gibson, N., Geiser, M., Wenk, A. (2011). Generation and characterization of stable, highly concentrated titanium dioxide nanoparticle aerosols for rodent inhalation studies. *J. Nanopart. Res.* 13, 511–524.

Lafont, U., Simonin, L., Tabrizi, N. S., Schmidt-Ott, A., and Kelder, E. M. (2009). Synthesis of nanoparticles of Cu, Sb, Sn, SnSb and Cu<sub>2</sub>Sb by densification and atomization process. *J. Nanosci. Nanotechnol.* 9, 2546–2552.

Lee, C., Rai, P., Moon, S., & Yu, Y. (2016). Thermal plasma synthesis of Si/SiC nanoparticles from silicon and activated carbon powders. *Ceramics International*, 42(15), 16469-16473.

Lee, S. J., Cho, J., Lee, C., Cho, J., Kim, Y., & Park, J. K. (2011). Synthesis of highly magnetic graphite-encapsulated FeCo nanoparticles using a hydrothermal process. *Nanotechnology*, 22(37), 375603.

Li, X., Meduri, P., Chen, X., Qi, W., Engelhard, M. H., Xu, W., Liu, J. (2012). Hollow core-shell structured porous Si-C nanocomposites for Li-ion battery anodes. *Journal of Materials Chemistry*, 22(22), 11014.

Li, Y., & Ishigaki, T. (2007). Synthesis and Structural Characterization of Core-Shell Si-SiC Composite Particles by Thermal Plasma In-Flight Carburization of Silicon Powder. *Journal of the Ceramic Society of Japan*, 115(1347), 717-723.

Lipp, L., & Pletcher, D. (1997). The preparation and characterization of tin dioxide coated titanium electrodes. *Electrochimica Acta*, 42(7), 1091-1099.

Liu, N., Wu, H., McDowell, M. T., Yao, Y., Wang, C., & Cui, Y. (2012). A Yolk-Shell Design for Stabilized and Scalable Li-Ion Battery Alloy Anodes. *Nano Letters*, 12(6), 3315-3321.

Liu, Z. J., Yuan, Z. Y., Zhou, W., Xu, Z., & Peng, L. M. (2001). Controlled Synthesis of Carbon-Encapsulated Co Nanoparticles by CVD. *Chemical Vapor Deposition*, 7(6), 248.

M. Zeng, L. Tan, J. Wang, L. Chen, M.H. Rummeli, L. Fu. (2014). Liquid metal: An innovative solution to uniform graphene films, *Chem. Mater.* 26, 3637–3643.

M.J. Assael, A.E. Kalyva, K.D. Antoniadis, R. Michael Banish, I. Egry, J. Wu, E. Kaschnitz, W.A. Wakeham. (2010). Reference data for the density and viscosity of liquid copper and liquid tin. *J. Phys. Chem. Ref. Data*. 39.

Majetich, S. A., Scott, J. H., Brunsmann, E. M., & Mchenry, M. E. (1994). Formation of Nanoparticles in A Carbon Arc. *MRS Proceedings*, 359.

Messing, M. E., Dick, K. A., Wallenberg, L. R., and Deppert, K. (2009). Generation of size selected gold nanoparticles by spark discharge for growth of epitaxial nanowires. *Gold Bull.* 42, 20–26.

Messing, M. E., Westerström, R., Meuller, B. O., Blomberg, S., Gustafson, J., Andersen, J. N. (2010). Generation of Pd model catalyst nanoparticles by

spark discharge. *J. Phys. Chem.* 114, 9257–9263.

Meuller, B. O., Messing, M. E., Engberg, D. L., Jansson, A. M., Johansson, L. I., Norlén, S. M., Deppert, K. (2012). Review of Spark Discharge Generators for Production of Nanoparticle Aerosols. *Aerosol Science and Technology*, 46(11), 1256-1270.

Miser, B. (2017). Production and characterization of carbon-silicon nanocomposite anode materials for secondary lithium batteries. (Doctoral dissertation). Retrieved from METU Theses Collection. (Accession No. 2550702031700212)

Nam, J. S., Hong, B., & Seo, J. (2013). Numerical Analysis on RF (Radio-frequency) Thermal Plasma Synthesis of Nano-sized Ni Metal. *Journal of the Korean Institute of Electrical and Electronic Material Engineers*, 26(5), 401-409.

Niu, J., Zhang, S., Niu, Y., Song, R., Song, H., Chen, X., & Hong, S. (2015). Towards Si@SiO<sub>2</sub> Core-shell, Yolk-shell, and SiO<sub>2</sub> Hollow Structures from Si Nanoparticles through a Self-templated Etching-deposition Process. *Procedia Engineering*, 102, 1903-1907.

Oh, S., Li, J., & Ishigaki, T. (2005). Nanocrystalline TiO<sub>2</sub> powders synthesized by in-flight oxidation of TiN in thermal plasma: Mechanisms of phase selection and particle morphology evolution. *Journal of Materials Research*, 20(02), 529-537.

Rahman, M., Song, G., Bhatt, A., Wong, Y. and Wen, C. (2015). Nanostructured Silicon Anodes for High-Performance Lithium-Ion Batteries. *Advanced Functional Materials*, 26(5), pp.647-678.

Roth, C., Ferron, G. A., Karg, E., Lentner, B., Schumann, G., Takenaka, S., & Heyder, J. (2004). Generation of Ultrafine Particles by Spark Discharging. *Aerosol Science and Technology*, 38(3), 228-235.

Saito, Y., Okuda, M., Yoshikawa, T., Kasuya, A., & Nishina, Y. (1994). Correlation between Volatility of Rare-Earth Metals and Encapsulation of Their Carbides in Carbon Nanocapsules. *The Journal of Physical Chemistry*, 98(27), 6696-6698.

Samal, S., Mukherjee, P. S., & Mukherjee, T. K. (2010). Thermal plasma processing of ilmenite: A review. *Mineral Processing and Extractive Metallurgy*, 119(2), 116-123.

Schwyn, S., Garwin, E., & Schmidt-Ott, A. (1988). Aerosol generation by spark discharge. *Journal of Aerosol Science*, 19(5), 639-642.

Seipenbusch, M., Weber, A. P., Schiel, A., and Kasper, G. (2003). Influence of the gas atmosphere on restructuring and sintering kinetics of nickel and platinum aerosol nanoparticle agglomerates. *J. Aerosol Sci.* 34, 1699–1709.

Selwyn, G., Herrmann, H., Park, J., & Henins, I. (2001). Materials Processing using an Atmospheric Pressure, RF-Generated Plasma Source. *Contributions to Plasma Physics*, 41(6), 610-619.

Seo, J., & Hong, B. (2012). Thermal Plasma Synthesis Of Nano-Sized Powders. *Nuclear Engineering and Technology*, 44(1), 9-20.

Seraphin, S., Zhou, D., & Jiao, J. (1996). Filling the carbon nanocages. *Journal of Applied Physics*, 80(4), 2097-2104.

Seshadri, R., Sen, R., Subbanna, G., Kannan, K., & Rao, C. (1994). Iron, cobalt and nickel nanoparticles encapsulated in carbon obtained by the arc evaporation of graphite with the metals. *Chemical Physics Letters*, 231(2-3), 308-313.

Shin, S., & Jang, J. (2007). Thiol containing polymer encapsulated magnetic nanoparticles as reusable and efficiently separable adsorbent for heavy metal ions. *Chemical Communications*, 2(41), 4230.

Si, P., Zhang, Z., Geng, D., You, C., Zhao, X., & Zhang, W. (2003). Synthesis and characteristics of carbon-coated iron and nickel nanocapsules produced by arc discharge in ethanol vapor. *Carbon*, 41(2), 247-251.

Sim, S., Oh, P., Park, S., & Cho, J. (2013). Critical Thickness of SiO<sub>2</sub> Coating

Layer on Core@Shell Bulk@Nanowire Si Anode Materials for Li-Ion Batteries. *Advanced Materials*, 25(32), 4498-4503.

Su, X., Wu, Q., Li, J., Xiao, X., Lott, A., Lu, W., Sheldon, B. and Wu, J. (2013). Silicon-Based Nanomaterials for Lithium-Ion Batteries: A Review. *Advanced Energy Materials*, 4(1), p.1300882.

Tabrizi, N. S., Ullmann, M., Vons, V. A., Lafont, U., & Schmidt-Ott, A. (2008). Generation of nanoparticles by spark discharge. *Journal of Nanoparticle Research*, 11(2), 315-332.

Tabrizi, N. S., Xu, Q., Pers, N. M., & Schmidt-Ott, A. (2009). Generation of mixed metallic nanoparticles from immiscible metals by spark discharge. *Journal of Nanoparticle Research*, 12(1), 247-259.

Tabrizi, N. S., Xu, Q., van der Pers, N. M., Lafont, U., and Schmidt-Ott, A. (2009). Synthesis of mixed metallic nanoparticles by spark discharge. *J. Nanopart. Res.* 11, 1209–1218.

Taylor, P. R., & Pirzada, S. A. (1994). Thermal plasma processing of materials: A review. *Advanced Performance Materials*, 1(1), 35-50.

Todorovic-Marković, B., Marković, Z., Mohai, I., Károly, Z., Gál, L., Föglein, K., Szépvölgyi, J. (2003). Efficient synthesis of fullerenes in RF thermal plasma reactor. *Chemical Physics Letters*, 378(3-4), 434-439.

Tomita, M., Saito, Y., & Hayashi, T. (1993). LaC<sub>2</sub> Encapsulated in Graphite Nano-Particle. *Japanese Journal of Applied Physics*, 32(Part 2, No. 2B).

Vons, V. A., Louis C. P. M. De Smet, Munao, D., Evirgen, A., Kelder, E. M., & Schmidt-Ott, A. (2011). Silicon nanoparticles produced by spark discharge. *Journal of Nanoparticle Research*, 13(10), 4867-4879.

Wozniak, M. J., Wozniak, P., Bystrzejewski, M., Cudzilo, S., Huczko, A., Jelen, P., Lewandowska-Szumiel, M. (2006). Magnetic nanoparticles of Fe and Nd-Fe-B alloy encapsulated in carbon shells for drug delivery systems: Study of the structure and interaction with the living cells. *Journal of Alloys and Compounds*, 423(1-2), 87-91.

Xuan, S., Hao, L., Jiang, W., Gong, X., Hu, Y., & Chen, Z. (2007). A facile method to fabricate carbon-encapsulated Fe<sub>3</sub>O<sub>4</sub> core/shell composites. *Nanotechnology*, 18(3), 035602.

Yin, Y., & Talapin, D. (2013). The chemistry of functional nanomaterials. *Chemical Society Reviews*, 42(7), 2484.

Yu, G., Sun, B., Pei, Y., Xie, S., Yan, S., Qiao, M., Zong, B. (2010). Fe<sub>x</sub>O<sub>y</sub>@C Spheres as an Excellent Catalyst for Fischer–Tropsch Synthesis. *Journal of the American Chemical Society*, 132(3), 935-937.

Zhang, H., Cao, T., & Cheng, Y. (2015). Preparation of few-layer graphene nanosheets by radio-frequency induction thermal plasma. *Carbon*, 86, 38-45.

Zhang, H., Liang, C., Liu, J., Tian, Z., & Shao, G. (2013). The formation of onion-like carbon-encapsulated cobalt carbide core/shell nanoparticles by the laser ablation of metallic cobalt in acetone. *Carbon*, 55, 108-115.

Zhang, T., Fu, L., Gao, J., Yang, L., Wu, Y., & Wu, H. (2006). Core-shell Si/C nanocomposite as anode material for lithium ion batteries. *Pure and Applied Chemistry*, 78(10), 1889-1896.

Zhou, X., Tang, J., Yang, J., Xie, J., & Ma, L. (2013). Silicon@carbon hollow core–shell heterostructures novel anode materials for lithium ion batteries. *Electrochimica Acta*, 87, 663-668.

Zuo, X., Zhu, J., Müller-Buschbaum, P., & Cheng, Y. (2017). Silicon based lithium-ion battery anodes: A chronicle perspective review. *Nano Energy*, 31, 113-143.